

CRoP: Context-wise Robust Static Human-Sensing Personalization

SAWINDER KAUR¹, AVERY GUMP², JINGYU XIN¹, YI XIAO⁴, HARSHIT SHARMA⁴, NINA R BENWAY³, JONATHAN L PRESTON¹, ASIF SALEKIN⁴

¹SYRACUSE UNIVERSITY ²UNIVERSITY OF WISCONSIN-MADISON ³UNIVERSITY OF MARYLAND-COLLEGE PARK ⁴ARIZONA STATE UNIVERSITY

The advancement in deep learning and internet-of-things have led to diverse human sensing applications. However, distinct patterns in human sensing, influenced by various factors or contexts, challenge the generic neural network model's performance due to natural distribution shifts. To address this, personalization tailors models to individual users. Yet most personalization studies overlook intra-user heterogeneity across contexts in sensory data, limiting intra-user generalizability. This limitation is especially critical in clinical applications, where limited data availability hampers both generalizability and personalization. Notably, intra-user sensing attributes are expected to change due to external factors such as treatment progression, further complicating the challenges. To address the intra-user generalization challenge, this work introduces CRoP, a novel static personalization approach. CRoP leverages off-the-shelf pre-trained models as generic starting points and captures user-specific traits through adaptive pruning on a minimal sub-network while preserving generic knowledge in the remaining parameters. CRoP demonstrates superior personalization effectiveness and intra-user robustness across four human-sensing datasets, including two from real-world health domains, underscoring its practical and social impact. Additionally, to support CRoP's generalization ability and design choices, we provide empirical justification through gradient inner product analysis, ablation studies, and comparisons against state-of-the-art baselines.

Additional Key Words and Phrases: Intra-user Generalization, Personalization, Contest-wise Robustness

ACM Reference Format:

Sawinder Kaur¹, Avery Gump², Jingyu Xin¹, Yi Xiao⁴, Harshit Sharma⁴, Nina R Benway³, Jonathan L Preston¹, Asif Salekin⁴,
¹Syracuse University ²University of Wisconsin-Madison ³University of Maryland-College Park ⁴Arizona State University . 2024. CRoP: Context-wise Robust Static Human-Sensing Personalization. 1, 1 (November 2024), 33 pages. <https://doi.org/10.1145/nnnnnnnn.nnnnnnnn>

1 INTRODUCTION

Recent automated human sensing applications—like activity recognition, fall detection, and health tracking – revolutionize daily life, especially in personal health management [85]. However, unique user patterns and natural distribution shifts [24] caused by behaviors, physical traits, environment, and device placements [73, 78] lead to the underperformance of generic sensing models in practical use. To tackle this, various domain adaptation techniques have been explored, with personalization widely used to adapt a generic model to the target user's specific domain or natural distribution [1, 9, 32, 39, 53, 62, 67]. In literature, personalization occurs either during the enrollment phase (static) [10, 15, 45] or continuously throughout application use, a process known as continual learning [13, 44, 87, 90].

Continual learning methods involve retraining models with new data, either supervised or unsupervised. While these approaches enable models to adapt to new patterns and changes in data distribution over time, they

Author's address: Sawinder Kaur¹, Avery Gump², Jingyu Xin¹, Yi Xiao⁴, Harshit Sharma⁴, Nina R Benway³, Jonathan L Preston¹, Asif Salekin⁴

¹Syracuse University ²University of Wisconsin-Madison ³University of Maryland-College Park ⁴Arizona State University.

Permission to make digital or hard copies of all or part of this work for personal or classroom use is granted without fee provided that copies are not made or distributed for profit or commercial advantage and that copies bear this notice and the full citation on the first page. Copyrights for components of this work owned by others than ACM must be honored. Abstracting with credit is permitted. To copy otherwise, or republish, to post on servers or to redistribute to lists, requires prior specific permission and/or a fee. Request permissions from permissions@acm.org.

© 2024 Association for Computing Machinery.

XXXX-XXXX/2024/11-ART \$15.00

<https://doi.org/10.1145/nnnnnnnn.nnnnnnnn>

often face efficiency challenges. As Harun et al. [28] points out, these methods, particularly those that prevent catastrophic forgetting [13, 19, 35, 50, 51, 74, 75, 87, 88], often struggle with memory, computation, and storage requirements inefficiencies, limiting their real-world applicability. Frequent model updates on user devices can introduce significant delays. This is especially true for devices with limited processing power, such as smartphones or wearables. These delays reduce the responsiveness of the application. They also lead to battery drain and inefficiency in real-time applications. Furthermore, to avoid catastrophic forgetting, several continual learning approaches rely on replay-based methods which require storage of previously encountered data [29, 80, 81]. This not only increases storage requirements but also raises privacy concerns. Constantly storing potentially identifiable information increases the risk of data breaches or misuse. This is especially concerning in regulatory environments, such as healthcare [83].

Additionally, supervised continual learning approaches face the significant challenge of requiring expert-labeled data for each new batch of user interactions, also termed as label delay [12]. This demand for continuous, high-quality labels can make it impractical for many applications, especially in settings where expert annotation is costly or unavailable. For example, in clinical or health monitoring contexts, each new data point may need to be validated by professionals, which is time-consuming and difficult to scale.

In contrast, static personalization offers an efficient alternative by customizing the model with a one-time, limited dataset collected during enrollment. This approach minimizes computation, requires no ongoing data or label storage or collection, and reduces user engagement, making it especially suitable for resource-constrained human-sensing applications. However, existing such studies often overlook intra-user variability due to factors like changes in magnetic field [63], sensor position [57], terrain [37], or the health symptoms [55], leading to poor intra-user generalizability for contexts not present during personalization. For instance, a smartphone activity recognition model personalized with handheld data may perform poorly when the phone is in a pocket.

Static personalization is particularly crucial for clinical datasets, which often suffer from data scarcity, leading to reduced robustness of lab-validated models for prospectively collected users [8]. It enhances model accuracy for clinical users whose traits are underrepresented in the global model's training data. In contrast, continuous supervised personalization is generally infeasible in many health domains since ground truths must be validated by clinicians, making it impractical in continuous settings, especially in remote or mobile health applications.

Notably, the distribution of clinical data is expected to shift, even within the same individual. For instance, in clinical speech technologies, changes in data distribution over time may occur due to the progression of neurodegenerative diseases, relevant for disease monitoring apps [72], or through desired learning mechanisms resulting from the use of technology, as seen in automated speech therapy apps [6]. Similarly, in wearable-based stress monitoring, psychophysiological data distribution varies as individuals face different stressors [54]. This research defines 'context' as the intra-user data distribution formed by varying factors.

This research gap is worsened since static personalization typically relies on a small sample set from the target user, covering limited contexts—particularly in clinical settings or applications with data scarcity [6, 8]. Commercial human sensing technologies like Google Assistant, Amazon Alexa, and Apple's Siri also statically personalize speech recognition models using limited phrases [4, 58, 77]. Similarly, the Apple Watch uses initial calibration for enhanced running activity tracking [2, 59]. This limited context during personalization is problematic, as shown in Section 3, where we demonstrate that static personalization may improve performance in training contexts but can also significantly degrade it in other unseen contexts for the same user.

Therefore, given the importance of static personalization in human sensing, this paper addresses its intra-user generalizability gap. Since personalized models are tailored to individual users and not intended for use by others, inter-user generalizability is outside the scope of this work. An additional challenge is that several personalization approaches in the literature, such as EMGSense [15] and MobilePhys [45], train their own generic models, sometimes even using data from target users. This limits privacy-preserving generic model sharing, and, in some cases, requires target users to share sensitive data, raising additional privacy concerns. It also complicates adding

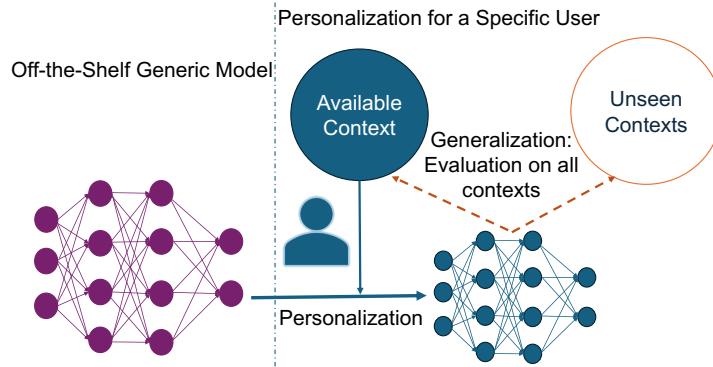


Fig. 1. Problem Setting

a new user, as the generic model must be updated and redistributed. While model redistribution is common in federated learning, human-sensing personalization isn't limited to federated learning methods. To address this limitation, this paper only uses pre-trained, off-the-shelf models as generic models, which do not require data from the target users.

In summary, Figure 1 outlines the paper's scope and objective. The goal is to develop an intra-user robust approach to personalize an off-the-shelf generic model for a specific user using limited data from limited contexts. The primary objective is to ensure that the personalized model thus obtained exhibits robust generalization capabilities across unseen contexts. Crucially, unseen context data takes no part in training or adjusting the personalized model outcome, and the generic model remains entirely off-the-shelf, with no accessibility for modification or design choices. These constraints highlight the real-world impact of this research, particularly in clinical settings where privacy concerns often limit data sharing [49, 61], and only trained off-the-shelf models are shared among researchers and developers.

To achieve the research objective in Figure 1, this paper introduces **CRoP**, a novel approach to create context-wise intra-user robust static personalized models. The key contributions are:

- (1) It facilitates utilizing readily available off-the-shelf pre-trained models with state-of-the-art accuracy, eliminating the need for training customized generic models, thus reducing training effort and providing a strong foundation for personalization.
- (2) Personalization with intra-user generalization has two challenges: i) learning user-specific patterns and ii) keeping information about generic patterns intact. During personalization, **CRoP** leverages pruning and regularization to capture the user-specific patterns present in the available-context data on a minimal sub-network of the model. The remaining parameters of the model are utilized to retain generic patterns that are not present in the available context, i.e., personalization data, thus achieving intra-user generalizability to unseen contexts. Pruning is widely used in other areas, including in continuous learning literature (e.g., Packnet [50], and Piggyback [51]), to obtain sub-networks for each new task which not only requires data from every task (here unseen context) but also needs identification of the task differences (i.e., difference among unseen contexts) in order to select the sub-network for inference. In contrast, this is the first paper to use pruning with adaptive intensity to capture the user's traits in a compressed sub-network, thus striking a balance between personalization and robustness in new, unseen contexts for the same user without identifying the contexts, their differences, or requiring data from unseen contexts for adaptation.

- (3) To showcase **CRoP**’s efficacy, comprehensive evaluations were performed on four human sensing datasets: PERCERT-R [7]: a clinical speech therapy dataset, WIDAR [94]: a lab-based WiFi-CSI dataset, ExtraSensory: a real-world mobile sensing dataset [79], and a stress-sensing dataset [91], while considering two disjoint contexts for each dataset. In order to obtain information about context variation within PERCEP-R and Stress-sensing, we collaborated with the original authors of these two datasets. This additional annotation will be released alongside this publication.
- (4) On an average across all datasets, **CRoP** shows a personalization benefit of 35.23 percent points and generalization benefit of 7.78 percent points. As compared to the best baseline (Packnet), these gains are 9.18 and 9.17 percent points higher, respectively. Moreover, alongside a detailed ablation study discussion in Section 8, an empirical justification of **CRoP**’s design choices that enable intra-user generalizability among different contexts is provided in Section 7.1, employing Gradient Inner Product(GIP) [70] analysis. Additionally, in order to demonstrate the feasibility of on-device personalization through **CRoP**, we compute training time and resource requirements for five platforms or devices.

The paper is arranged in different sections. Section 2 reviews the related work, while Section 3 presents the results of a preliminary study on the WIDAR datasets, which motivates the proposed approach. Section 4 provides a formal description of the problem statement, followed by Section 5, which outlines the detailed methodology. Section 6 covers the experimental setup, and results. In Section 7, we present an empirical study to justify the approach, and Section 8 offers an ablation study to support various design choices. Section 9 discusses runtime analysis, Section 10 explores limitations and future directions, and Section 11 addresses the broader impact of the work. Finally, Section 12 concludes the study.

The work is accompanied by an extensive appendix, which provides details of experiment setup, hyperparameters, and link to code ensuring reproducibility in Appendix A. Additionally, Appendix B provides a detailed analysis of the user-specific results for each dataset along with a detailed ablation study.

2 RELATED WORK

As discussed above, this work aims to personalize off-the-shelf models while ensuring intra-user generalizability leveraging limited-context data. While existing approaches attempt to address these adaptation challenges, they often impose restrictive conditions. Many require specialized training of the generic model with access to the generic data, assume knowledge of the target domain, or necessitate target users to share their data from a new/previous-unseen context for adapting the model, in some studies with labels or annotations. Additionally, some methods rely on repetitive model retraining, which hinders their suitability for real-world applications due to privacy concerns, computational inefficiency, or excessive user engagement.

This section summarizes and critiques key state-of-the-art approaches with similar objectives to those addressed in this work, highlighting their contributions and limitations in practical, user-centered adaptation settings.

2.1 Domain Adaptation and Generalization

Domain adaptation (DA) and Domain Generalization (DG) techniques address performance drops due to distributional shifts between source and target domains [36]. These methods are useful when models trained on generic data need to adapt to new users or contexts. The key difference is that while DA approaches have access to target domain data, DG techniques work without any target domain data, not even unlabeled [86].

The domain generalization techniques can be categorized into Data Manipulation, Representation Learning, and other learning strategies [86]. Data Manipulation approaches include techniques like data augmentation and synthetic data generation, which are used to increase data diversity, helping models learn invariant features across different domains [68, 84, 95]. Representation Learning aims to capture domain-invariant features using techniques like adversarial training and embedding learning to improve model robustness, such as Invariant

risk minimization (IRM)[3] and domain-adversarial neural networks (DANN)[22]. Learning Strategies such as meta-learning [41] and ensemble learning [14] train the model on multiple simulated domains to improve its ability to generalize. However, all of these approaches aim to train the generic model while this paper's scope does not allow access to generic data and uses a pre-trained off-the-shelf model for adaptation.

Similarly, some domain adaptation approaches rely on generic model training while utilizing data from the target domain [47]. On the other hand, certain domain adaptation approaches require access to the source data used to train the generic model without requiring specialized training of the generic model. These approaches rely on discrepancy minimization and self-supervision to align source and target distributions by learning domain-invariant representations [21, 42]. A few approaches that do not require access to the source domain data or generic model training are referred to as source-free domain adaptation (SFDA)[43]. Liang et al. [43] (SHOT) proposed the transfer of hypothesis from source by freezing the parameter weights for the classifier layers and only allowing the feature extraction layer to be finetuned to the new domain. The approach is applicable to unsupervised domain adaptation scenarios and employs self-supervised pseudo-labeling to align the target domain's representations to the source hypothesis.

Given that the problem addressed by SHOT aligns with the criteria of having no access to generic data and avoiding specialized generic model training, we adopted SHOT as one of the baseline approaches in this study. However, it is important to note that SHOT does not effectively tackle the limitations posed by restricted-context data during the fine-tuning process. As a result, its performance may not adequately generalize to the intra-user variability present in the data, which is a crucial aspect of our research focus.

2.2 Continual Learning

Continual personalization approaches [13, 19, 50, 51, 74, 75, 87, 88] can improve intra-user generalizability by continually fine-tuning the model as new data arrives. Some of these approaches [19, 74, 75] require specialized training of the generic model, limiting the use of off-the-shelf pre-trained models. Others like PackNet [50] and Piggyback [51] propose supervised methods that require continued stream of labeled data, limiting their application in health-care scenarios. However, all continuous learning approaches require repeated computation overhead to adjust the model outcome to new data [60], which can be infeasible in real-time applications, more so for scalable platforms like wearables [65], which is prominent for health sensing such as stress or fall detection. Daniels et al. [13] proposes a continual training framework that is compatible with edge devices and requires less training effort, but it uses a different and smaller model architecture at the personalized devices for generating feature embeddings. Thus hindering the direct usage of off-the-shelf models and increasing the training effort. Nevertheless, since the problems addressed by Packnet, and Piggyback are the closest to the problem addressed in this study, we considered these approaches as baselines.

Packnet [50] and Piggyback [51] adapt the generic model for a stream of continuously changing tasks. Packnet relies on finetuning, pruning and re-training the model for each new task. On the other hand, Piggyback employs pruning to learn a new binary mask for each new task which is then applied to a generic model in order to get task-specific results. However, this requires correct identification of the task before choosing the mask. For every new task, the same procedure is repeated, hoping that different sets of parameters will be important for different tasks. This aligns well with our initial study, where we identify that different contexts' data focus on different sets of parameters.

Notably, all continual learning approaches, including PackNet and Piggyback, face a significant limitation: they necessitate access to data from the target domain, whether in a supervised or unsupervised format, in order to effectively adapt the model. While these approaches successfully address the challenge of catastrophic forgetting, they primarily focus on contexts that the model has previously encountered, leaving them ill-equipped to adapt to entirely unseen domains. In contrast, our research framework specifically excludes access to data from these

unseen contexts during model adaptation, highlighting a critical gap in the capabilities of existing continual learning methodologies. Consequently, PackNet, Piggyback, and similar approaches lack the mechanisms necessary to adapt to novel domains, underscoring the need for innovative strategies that can operate without prior exposure to the target data.

2.3 Test-Time Adaptation (TTA)

Continual learning requires repeated training cycles to adapt models to new information, demanding high computational resources, storage, and long-term data retention, which raises privacy concerns [83]. This makes traditional continual learning impractical for sensitive domains like healthcare [28].

Test-time adaptation offers a more efficient and flexible alternative, allowing models to adapt in real-time during deployment by making adjustments based on incoming data without necessitating a complete retraining process. By focusing on adapting the model in real-time, test-time adaptation minimizes resource consumption as compared to continual learning approaches. Wang et al. [87] relies on generating pseudo-labels using weighted averaging and augmentation-averaged predictions, which can introduce bias [43]. While Wu et al. [90] achieves test-time domain adaptation by manipulating batch-normalization layers, thus enforcing a restriction on model architecture. However, Continual Test Time Domain Adaptation (CoTTA) [88] does not have such restrictions and allows the use of off-the-shelf models.

CoTTA [88] is an unsupervised learning approach designed to enhance model adaptation in dynamic environments. It utilizes a teacher model, which is initially set up as a replica of the generic model, to generate pseudo-labels for training. During each iteration, the teacher model is updated using current model state through a weighted sum, allowing the model to effectively account for evolving data patterns over time. Additionally, the current model state is subject to a stochastic restoration of weights, implemented through a Bernoulli distribution with a very low probability of success. This randomization introduces an element of variability that helps prevent overfitting and encourages exploration of the weight space, further enhancing the model's ability to generalize to unseen data.

Since CoTTA addresses a problem setting similar to ours, we adopt it as one of our baseline approaches. In our setup, data from the available context can be leveraged for test-time adaptation, while unseen context data is reserved solely for empirical evaluation. However, test-time adaptation methods, including CoTTA, tend to increase resource demands during inference, leading to potential delays that can impact real-time usability. This additional computational overhead highlights a key limitation of test-time adaptation in applications where real-time response is essential.

2.4 Personalization Approaches

A few static personalization approaches [10, 15, 45] aimed for the additional goal of out-of-distribution robustness. However, these methods require access to the generic model—either to make specific design choices [10], which prevents them from utilizing off-the-shelf models, or to incorporate knowledge about the target user's data distribution during the generic model's training phase [15, 45], raising privacy concerns, particularly in sensitive clinical applications. These requirements do not align with the research objectives of this paper, making them unsuitable as baselines.

For instance, EMGSense [15] is concerned with robustness to distributional shifts in Surface Electromyography (EMG) signals caused by the heterogeneity of biological factors across users. The generic model consists of a multi-model voting ensemble DNN that needs to be trained on N source distributions and some unlabeled data from target users. To learn user-specific features, this model undergoes multiple training iterations, each using updated user-specific data.

Feature → Approach ↓	Off-the-shelf Generic model	Generic Data unseen	Adaptation to available context	Robustness to unseen Context
Arjovsky et al. [3], Ganin et al. [22]	✗	✗	-NA-	✓
Long et al. [47]	✗	✗	✓	✗
Ganin and Lempitsky [21], Li et al. [42]	✓	✗	✓	✗
SHOT [43]	✓	✓	✓	✗
Packnet[50] and Piggyback[51]	✓	✓	✓	✗
COTTA [88]	✓	✓	✓	✗
EMGSense [15] and MobilePhys [45]	✗	✗	✓	✗
PTN [10]	✓	✓	✓	✗
CRoP	✓	✓	✓	✓

Table 1. Summary of Literature review

Also, MobilePhys [45] addresses distributional shifts that can arise due to environmental conditions (e.g., lighting, motion) as well as individual physiological and visual (e.g., clothing, posture) differences in camera-based contactless Photoplethysmography. The generic model is trained using meta-learning, which uses data from target users to enable quick adaptation to distributional shifts during personalization.

Consequently, the major drawback faced by EMGSense[15] and MobilePhys [45] is the requirement of knowledge of the target user’s data in order to train the generic model. This necessitates the transfer of the user’s unlabelled data from the user’s device to a central server. Such data can contain sensitive information, and thus, its transfer suffers from legal and regulatory barriers [20]. More importantly, since the training of the generic model requires a subset of each target user’s unlabelled data, the introduction of any new user will require re-training of the generic model and its distribution, which is an overhead.

Recently, Burns et al. [10] extends the idea of triplet loss [66] to the task of personalization (PTN). The optimization objective combines the minimization of the Euclidean distance between data from the same target classes while maximizing the Euclidean distance between different target classes in order to learn an embedding optimized for the desired task. The features extracted using DNN have been shown to be superior to the engineered features [64]. Thus, Burns et al. [10] uses these features to train a KNN for the final prediction task. The approach has been shown to be robust for out-of-distribution data.

However, none of these approaches address intra-user variability in data. Since PTN allows the usage of off-the-shelf model and does not require sharing of the personal data for generic model training, we consider PTN as one of the baselines.

2.5 Selecting Baselines

The problem addressed in this work has the following requirements: using an Off-the-shelf generic model, having no access to the generic data, and requiring adaptation to available context data and robustness to unseen data. As discussed in the previous sections and summarized in Table 1, the approaches SHOT [43], PTN [10], PackNet [50], Piggyback [51], and Continual Test Time Domain Adaptation (CoTTA) [88] comply with the first three requirements. Thus, we adapt these approaches to the problem statement addressed in this work and use them as our baselines. These approaches typically rely on training data from a specific context to adapt to that context. However, the scenario addressed in this work limits training data to only one context, with the expectation that the approach will also perform well in unseen contexts. Since data from unseen contexts is unavailable, we prevent these approaches from using it during training. Instead, the data used for training or adaptation is restricted to data belonging to the available context only, while the unseen context data is used merely for testing.

(a) Context C1						(b) Context C2							
Model	Generic		Personalized		Δ		Model	Generic		Personalized		Δ	
User	C1	C2	C1	C2	C1	C2	User	C1	C2	C1	C2	C1	C2
0	63.90	77.09	87.06	65.02	+23.16	-11.88	0	60.80	73.28	57.46	77.30	-3.34	+4.02
1	61.80	79.78	89.38	44.38	+27.57	-35.40	1	59.58	73.18	42.38	93.75	-17.29	+20.57
2	45.63	79.81	71.88	64.45	+29.75	-26.62	2	46.13	80.46	40.19	87.15	-5.93	+6.69
Average					+26.82	-24.63	Average					-8.85	+10.43

Table 2. Performance Comparison in terms of inference accuracy of Generic model with conventionally trained personalized model

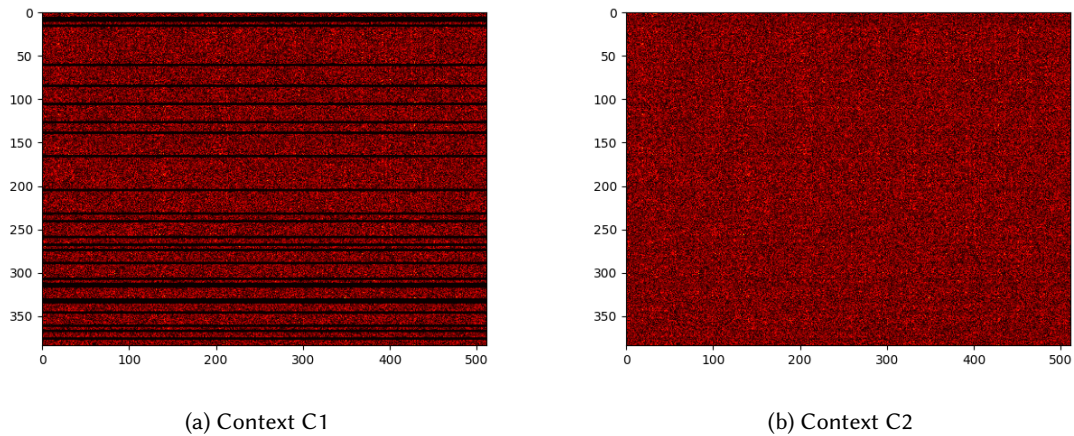


Fig. 2. Heat map for the absolute magnitude of parameters belonging to penultimate layer for LeNet models finetuned using data from context (a) C1 and (b) C2

3 MOTIVATION

When learning patterns from human sensing data in a limited context, conventional fine-tuning approaches can overwrite generic knowledge that is not relevant to that specific context but applicable to others, leading to a performance drop in those unrepresented contexts. To illustrate this, we conducted a preliminary study comparing the performance of generic and *conventionally-finetuned* [31] personalized human-gesture-recognition models using the LeNet architecture [94] trained on the WIDAR dataset. Data preprocessing details are discussed in the Section 6 (Experiments).

Table 2a compares the performance of generic and *conventionally-finetuned* [31] personalized models on each user’s data belonging to context C1 and evaluated to the same user’s disjoint data in both C1 (available) and C2 (unseen) contexts. It can be observed that conventional finetuning introduces a significant gain of 26.82% for context C1’s data but at the cost of 24.63% reduction in context C2. Similar patterns are seen when personalization is performed on context C2 as shown in Table 2b. Thus, conventional finetuning-based personalization of the models using the limited data from one context can significantly worsen the model’s performance in an unseen context.

To investigate this discrepancy in performance, we compare the distribution of parameter magnitudes of the models personalized on contexts C1 and C2 using *conventional finetuning*, as shown using heat maps in Figures

2 (a) and 2 (b). Notably, there is a substantial difference in parameter magnitudes between models trained in different contexts. Additionally, the parameters represented by black pixels in Figure 2 have magnitudes close to zero, indicating two crucial aspects: **(a)** Their contribution to model inference is negligible, implying redundancy. **(b)** Interestingly, some of these parameters have high magnitudes in the personalized model of another context, indicating that parameters considered unimportant in one context may be crucial in another.

The critical question arises: *How can we effectively retain and transfer the valuable generic information about unseen contexts (e.g., one of the unseen contexts is C_2 in the above example) to the personalized models without access to the unseen contexts?* – that this paper addresses.

4 PROBLEM STATEMENT

Given a generic model \mathcal{M}_θ^G , the objective is to tailor a personalized model $\mathcal{M}_\theta^{P_i^a}$ specifically for a user \mathcal{U}_i utilizing the data \mathcal{D}_i^a associated with available context C_a , here θ represents the parameters of the model. The primary goal is to ensure that the personalized model $\mathcal{M}_\theta^{P_i^a}$ performs reasonably well on \mathcal{U}_i 's data \mathcal{D}_i^u derived from unseen contexts C_u . Notably, there is no overlap between the data belonging to the available and unseen contexts, that is, $\mathcal{D}_i^a \cap \mathcal{D}_i^u = \emptyset$.

In other words, if $\mathcal{M}_\theta^{C_i^a}$ represents a *conventionally-finetuned* model trained for a user \mathcal{U}_i on data \mathcal{D}_i^a , then, the models trained using CRoP, $\mathcal{M}_\theta^{P_i^a}$, must on avg. perform better on both available C_a and unseen context C_u than $\mathcal{M}_\theta^{C_i^a}$. More formally, the learning objective can be defined as:

$$\mathcal{M}_\theta^{P_i^a} = \underset{\theta}{\operatorname{argmin}} \sum_{d \in \mathcal{D}_i^a} \ell(\mathcal{M}_\theta^G, d),$$

such that $\mathcal{D}_i^a \cap \mathcal{D}_i^u = \emptyset$ and

$$\sum_{d \in \{\mathcal{D}_i^u, \mathcal{D}_i^a\}} \ell(\mathcal{M}_\theta^{P_i^a}, d) < \sum_{d \in \{\mathcal{D}_i^u, \mathcal{D}_i^a\}} \ell(\mathcal{M}_\theta^{C_i^a}, d),$$

that is, the loss incurred by the resulting personalized model $\mathcal{M}_\theta^{P_i^a}$ on avg. across all contexts' data is less than the loss incurred by *conventionally-finetuned* model $\mathcal{M}_\theta^{C_i^a}$. Here, ℓ represents the standard cross-entropy loss.

It is important to emphasize that the above-mentioned optimization problem restricts the usage of data only to the available context C_a and has no knowledge of data from the unseen context C_u . Hence, for $d \in \mathcal{D}_i^u$ (unseen context data), the information $\ell(\mathcal{M}_\theta^{P_i^a}, d)$, and $\ell(\mathcal{M}_\theta^{C_i^a}, d)$ is absent during the training process.

5 APPROACH

5.1 Rationale for The CRoP Approach Design

As previously discussed, the generic model's parameters contain generalizable information across all contexts. Addressing the problem statement requires retaining this information to the greatest extent while enabling fine-tuning for the target user. Furthermore, our investigation revealed that different parameters hold varying degrees of importance in distinct contexts. Hence, the careful selection of subsets of model parameters for personalization and generalization is pivotal for the success of the approach, for which this paper leverages the model pruning paradigm.

Model pruning is based on the idea that neural networks include redundant parameters, and removing these parameters minimally impacts the model's performance [48, 96]. Consequently, pruning the fine-tuned personalized model ensures the retention of essential parameters to maintain accuracy for context C_a , meaning, capturing the target user-specific traits. However, the pruned parameters can be replaced with corresponding parameters from the generic model, effectively restoring generic knowledge learned across all contexts on those

Algorithm 1 CRoP

1: **Input:** \mathcal{M}_θ^G : Generic Model $\diamond \mathcal{D}_i^a$: User \mathcal{U}_i 's data for available context C_a $\diamond \alpha$: coefficient of regularization
 $\diamond \tau$: tolerance for pruning

2: Train the Generic model on the personal data \mathcal{D}_i^a

$$\mathcal{M}_{\theta'}^{P_i^a} = \underset{\theta}{\operatorname{argmin}} \sum_{d \in \mathcal{D}_i^a} \ell(\mathcal{M}_\theta^G, d) + \alpha \|\mathcal{M}_\theta^G\|_1$$

3: Prune redundant parameters to obtain the pruned sub-structure

$$\mathcal{M}_{\theta'}^{P_i^a} = \text{ToleratedPrune}(\mathcal{M}_{\theta'}^{P_i^a}, \tau)$$

4: Copy the parameters of generic models to the pruned parameters in the personalized pruned model,

$$\mathcal{M}_{\theta''}^{P_i^a} = \begin{cases} \mathcal{M}_{\theta'}^{P_i^a} & , \theta' \neq 0 \\ \mathcal{M}_\theta^G & , \text{otherwise} \end{cases}$$

5: Finetune the personalized model on the \mathcal{D}_i^a using early stopping with validation accuracy in C_a

$$\mathcal{M}_\theta^{P_i^a} = \underset{\theta}{\operatorname{argmin}} \sum_{d \in \mathcal{D}_i^a} \ell(\mathcal{M}_{\theta''}^{P_i^a}, d) + \alpha \|\mathcal{M}_{\theta''}^{P_i^a}\|_1,$$

generic model parameters. This restoration may enhance generalizability, ensuring robust performance in unseen contexts C_u . The approach presented in this paper is founded on this insightful strategy.

5.2 CRoP Approach

Algorithm 1 describes the presented approach, which takes as input: the generic model \mathcal{M}_G , user \mathcal{U}_i 's data \mathcal{D}_i^a for available context C_a , the initial value for the coefficient of regularization α and tolerance for pruning τ ; and generates the target personalized model $\mathcal{M}_\theta^{P_i^a}$. Here, α and τ are hyperparameters whose values can be tuned for the given data and model.

The approach initiates by finetuning the generic model \mathcal{M}_θ^G on data \mathcal{D}_i^a , concurrently applying ℓ_1 regularization to penalize model parameters (line 2). This regularization encourages sparsity by specifically targeting the magnitude of redundant parameters [52]. This step is followed by the pruning of redundant weights using the 'ToleratedPrune' module (line 3). The pruned weights are then replaced by the corresponding weights from the generic model \mathcal{M}_G (line 4) to restore generalizability; this hybrid model is referred to as the 'Mixed Model.' This step leads to the modification of the activated paths in the personalized model, resulting in changes in the model inferences. However, since the newly activated paths are determined by weights retained from two models and not learned from data patterns, there is a consequent loss of accuracy, as shown and discussed in Section 7.2. To mitigate such a loss, as a final step, the *Mixed Model* undergoes fine-tuning once again on the data from the available context \mathcal{D}_i^a (line 5). The detailed explanation of each of these steps is as follows:

Personalized Finetuning with Penalty (Algorithm 1 – Step 2): The approach uses data \mathcal{D}_i^a to finetune the generic model \mathcal{M}_θ^G . As shown in the Section 3 (Motivation), such conventional finetuning enhances the model's accuracy within the available context C_a . Nevertheless, its performance in unfamiliar contexts may get suboptimal. Notably, during the model's fine-tuning process, we apply ℓ_1 regularization to penalize the model weights, forcing the magnitudes of redundant parameters to be close to zero [52]. The regularization coefficient α is a trainable

Algorithm 2 ToleratedPrune($\mathcal{M}, \tau, \mathcal{D}$)

```

1: Input:  $\mathcal{M}_\theta$ : A Model ◊  $\tau$ : tolerance for pruning ◊  $\mathcal{D}$ : data
2: Pruning Amount  $p = k$ 
3:  $A_o = \text{accuracy}(\mathcal{M}_\theta, \mathcal{D})$ 
4: repeat
5:    $\mathcal{M}_{\theta \downarrow} = \mathcal{M}_\theta$ 
6:    $\mathcal{M}_\theta = \text{Prune}(\mathcal{M}_\theta, p)$ 
7:    $A = \text{accuracy}(\mathcal{M}_\theta, \mathcal{D})$ 
8:   Increment Pruning Amount  $p = p + k'$ 
9: until  $A < A_o - \tau$ 
10: return  $\mathcal{M}_{\theta \downarrow}$ 

```

parameter optimized during training to minimize the overall loss. As a result, the parameters with high magnitudes carry most of the information regarding the data patterns in \mathcal{D}_i^a , offering two key benefits:

- (1) Minimal loss in C_a accuracy: A high fraction of parameters have close to zero magnitudes, and their removal results in minimal information loss for context C_a ; thus, the adverse impact of pruning in context C_a is minimized.
- (2) Maximal generalization: The inclusion of regularization aids *ToleratedPrune* (discussed below) module in efficiently pruning a higher number of parameters, which are then replaced with weights from the generic model. This restores information from the generic model, contributing to enhanced accuracy in unseen contexts.

ToleratedPrune Module (Algorithm 1 – Step 3): Algorithm 2 outlines the *ToleratedPrune* module, taking a model \mathcal{M}_θ , pruning tolerance τ , and the dataset \mathcal{D} as inputs. It initiates with a modest pruning amount of k and incrementally increases this amount by k' until the model's accuracy exhibits a drop of τ percent on \mathcal{D} . Here, k and k' are hyperparameters within the range of $(0, 1)$. The module returns $\mathcal{M}_{\theta \downarrow}$, representing the pruned state of the model before the last pruning iteration. This state is such that further pruning would result in a higher accuracy loss on dataset \mathcal{D} than the tolerable amount τ . This module performs pruning leveraging the conventional magnitude-based unstructured pruning [96].

Thus, step 3 in Algorithm 1 generates a pruned personalized model state $\mathcal{M}_{\theta \downarrow}^{P_i^a}$ whose prediction accuracy on context C_a is at most τ percent lower than that of the earlier state $\mathcal{M}_{\theta'}^{P_i^a}$ while using only a fraction of its original parameters. The non-zero weights corresponding to these parameters contribute significantly to model inference for the available context C_a . As a result, $\mathcal{M}_{\theta \downarrow}^{P_i^a}$ is essentially the *minimal sub-structure* of the earlier state model $\mathcal{M}_{\theta'}^{P_i^a}$, which is crucial for correct inference for context C_a . This enables replacing a maximal number of zeroed-out parameters to incorporate information from unseen contexts using the generic model \mathcal{M}_θ^G in the subsequent steps.

Generating the Mixed Model (Algorithm 1 – Steps 4&5): For generating the *Mixed Model* $\mathcal{M}_{\theta''}^{P_i^a}$, the zeroed out parameters in the pruned model $\mathcal{M}_{\theta \downarrow}^{P_i^a}$ are replaced by the corresponding parameters in the generic model \mathcal{M}_θ^G , enabling generic knowledge restoration.

Notably, model pruning is often followed by a finetuning step [46, 48, 96], where the pruned model undergoes re-training to recover the performance lost during the pruning process. We have observed that, despite the *Mixed Model* exhibiting improved performance in the unseen context, there is a notable loss of accuracy in the available

context due to inconsistent activated paths, as discussed earlier. Thus, the resulting *Mixed Model* is fine-tuned using the available data \mathcal{D}_i^a . Goyal et al. [25] suggests that fine-tuning process should mirror pre-training for effective generalization. Therefore, our fine-tuning objective aligns with the pre-training objective used in Line 2 for optimal results.

During finetuning, the model state, including the *mixed model*, with the best validation loss on the seen context, is selected. We found that for some individuals, the *mixed model* is chosen as the optimal model, which indicates that for some individuals, further finetuning is not required, and our approach can automatically handle that scenario.

6 EXPERIMENTS

This section displays the empirical efficacy of the presented approach. Section 6.1 provides a detailed discussion of the four human sensing datasets and their pre-processing used in our evaluations: PERCEPT-R [7], WIDAR [94], ExtraSensory [79] and a Stress-sensing dataset [91], and also explains the corresponding model architectures as used in literature. Section 6.2 details the metrics of evaluation used in this work along with their practical relevance. This is followed by a detailed discussion of the empirical comparison of **CRoP** with five baselines SHOT[43], Packnet[50], Piggyback[51], CTTa[88] and PTN[10] in Section 6.3. Additionally, detailed discussions about interesting patterns, such as the impact of generic model quality on personalization, etc., are also provided.

Notably, each dataset offers a varying distribution of data among different classes, necessitating different performance metrics like inference accuracy and F1 score. For each dataset, our evaluation stayed aligned with the metrics previously used in studies evaluated on these datasets, with further details available in the Appendix A. Additional details to support reproducibility, such as hyperparameters, links to the code, and computation resources utilized, are also provided in Appendix A.

6.1 Datasets and models

This work employs four real-world human-sensing datasets to demonstrate the empirical efficacy of **CRoP**, two of which are associated with health applications. First, the PERCEPT-R dataset has been used for binary classification for predicting the correctness of /ɹ/ sounds in automated speech therapy application [6]. Additionally, we use the Stress Sensing dataset [91] collected using a psycho-physiological wrist-band, named Empatica E4 [17]. To further demonstrate the efficacy of **CRoP**, we incorporate two benchmark human-sensing datasets, which include data from the same individuals across multiple contexts: WIDAR [94] and ExtraSensory [79]. Specifically, we employ WIDAR for a 6-class classification focusing on gesture recognition using WiFi signals, and ExtraSensory for binary classification related to human activity recognition using accelerometer and gyroscope readings. Details on the datasets, preprocessing for personalized evaluations, and generic model training are discussed below.

PERCEPT-R: The sound /ɹ/ has been recognized as the most frequently impacted sound in residual speech sound disorders in American English [40] and considered to be the most difficult sound to treat. The PERCEPT-R Corpus was collected during 34 different cross-sectional and longitudinal studies of speech [7] for automated speech analysis of /ɹ/. The data used in this study come from the prospectively collected [6], and corpus version 2.2.2, which includes both the publicly available open access subset (2.2.2p) and privately held data that was not published in the open access subset after a review of consent/assent permissions. Items in the PERCEPT-R Corpus v2.2.2 primarily consist of single-word speech audio collected during clinical trials involving children with speech sound disorders affecting /ɹ/, along with age-matched peers with typical speech. The full corpus contains 179,076 labeled utterances representing 662 single-rhotic words and phrases. Each audio file is paired with a ground-truth label representing listener judgments of rhoticity, derived by averaging binary ratings (0 = derhotic, 1 = fully rhotic) from multiple listeners. For this study, the heuristic threshold for converting these averaged ratings into binary ground-truth labels was 0.66.

To use this dataset for our personalization evaluation, we collaborated with clinical experts to identify and acquire annotations of 16 participants who had correct and incorrect pronunciations of /ɪ/ sound at pre-treatment (baseline-phase) and during different treatment phases. As outlined in Section 4, the evaluation treats pre-treatment data as available context data, while data from other treatment phases serve as unseen context data.

WIDAR: WIDAR is a dataset collected for the purpose of gesture recognition. It was collected using off-the-shelf WiFi links (one transmitter and at least 3 receivers). 17 users performed 15 different gestures at different rooms and orientations (of the person). The channel state information is collected from these devices with amplitude noises and phase offsets removed as a preprocessing step. The two contexts used for the current work are decided based on the orientations of the torso data and room ID. Room 1 is a classroom with a number of objects (e.g., desks and chairs) in it, and Room 2 is a nearly empty hallway. The dissimilar data distributions can be attributed to the differences in the amount of interruptions in WiFi signals. We followed the same normalization methods as Yang et al. [92].

ExtraSensory: ExtraSensory is a human activity recognition dataset collected using the ExtraSensory mobile application. A number of features were collected from different cellular devices and smartwatches, though we just used the accelerometer and gyroscope features obtained from the cellular devices. Labels for activities were self-reported by the users through the mobile application. For our evaluations on ExtraSensory, 5 users were left out of training a single generic model. The contexts are decided based on the location of the phone: hand, pocket, and bag.

Stress Sensing Dataset: This dataset measures the physiological impacts of various kinds of Stress. The dataset is collected using Empatica E4 Wristband to extract features such as EDA (Electrodermal Activity), a skin temperature sensor (4 Hz), etc, contributing to a total of 34 features. The data was collected from 30 participants with different demographics, who were assigned the labels ‘Stressed’ or ‘Calm’ based on the different stress-inducing or calming tasks they experienced. In order to adapt this dataset for the problem addressed in this work, we collaborated with the original authors to identify participants who wore wristbands on both hands, which were then chosen for the task of personalization. Additionally, during the data collection, participants were asked to perform several activities, a few of which restricted participants’ movement while others allowed them to move. Based on this, the data was annotated with movement patterns, that is, still vs. moving. This additional annotation of the dataset will be made public along with this work. During this dataset’s evaluation, the context is defined by a combination of the hand on which the wristband was worn and whether or not the person was moving during the data collection.

6.1.1 Pre-Processing of the Datasets. We partitioned each dataset into two disjoint sets of users: (1) a generic dataset for training a generic model and (2) a personalized dataset for training a personalized model for each user. To demonstrate the context-wise robustness, we further partitioned each user’s (belonging to the later set) personalized dataset into different contexts (i.e., available C_a and unseen context C_u). Table 3 presents the details of this partitioning. For PRECEPT-R, we consider data from the pre-treatment phase as the available context, and the treatment phases, where participants undergo clinical interventions, are considered the unseen context. For the Stress Sensing dataset, the context is determined by two factors: the hand on which the sensor (Empatica E4 wristband [17]) was worn during data collection and the movement status of the individual. For WIDAR, context is determined by the room and torso orientation during data collection, while for the ExtraSensory dataset, phone’s location on the user’s body (e.g., hand, pocket, bag) defines the context. The term ‘Scenario’ refers to the combination of available C_a and unseen C_u contexts as outlined in Table 3. All datasets, along with context-wise annotations, will be made public.

Notably, throughout the training of personalized models, CRoP refrains from utilizing any information from the unseen context C_u . Therefore, while the empirical study indicates an enhancement in the model’s performance for

Dataset →	PERCEPT-R	WIDAR	ExtraSensory	Stress Sensing
Total users	515	17	60	30
Users' ID for Personalization	17,25,28,336,344,361,362,55, 586,587,589,590,591,61,67,80	0,1,2	80,9D,B7,61,7C	1,2,3
Scenario 1	C_a : Baseline Study C_u : Treatment Phase	C_a : Room-1, Torso Orientation- 1,2,3 C_u : Room 2, Torso Orientation- 4,5	C_a : Hand, Pocket C_u : Bag	C_a : Left hand, Still C_u^1 : Right hand, Still; C_u^2 : Right hand, Moving
Scenario 2	-N/A-	C_a : Room 2, Torso Orientation- 4,5 C_u : Room-1, Torso Orientation- 1,2,3	C_a : Bag, Pocket C_u : Hand	C_a : Right hand, Moving C_u^1 : Left hand, Moving; C_u^2 : Left hand, Still

Table 3. Details of data used for personalization

one or a few unseen contexts, it is a proxy for all unseen contexts. This means that it is reasonable to anticipate a favorable performance in other unseen contexts that are not available on the dataset.

Notably, the stress sensing dataset has been evaluated across two different unseen context variations. In C_u^1 , there was one change in context—a change in hand while keeping the same movement pattern as C_a . In C_u^2 , there were two changes—a change in both hand and movement patterns.

6.1.2 Training of the Generic models.

PERCEPT-R : For the identified 16 participants for our personalization evaluation, their speech data were collected longitudinally, meaning their data could be separated into available and unseen contexts versus other speakers in the corpus who only had speech data available from a one-time point. The generic model is trained for the remaining 499 participants (having /ɪ/ sounds disorder) using person-disjoint validation and test sets. The aim of this dataset is to identify the correctness of /ɪ/ sounds.

Model: In line with the literature Benway et al. [7], we tried several model architectures such as CNN, DNN, BiLSTM, etc, whose number of parameters were identified using grid search. Among those, the biLSTM model containing 4 bidirectional LSTM layers followed by 5 linear layers, accompanied by a Hardswish activation layer, was identified as the one that exhibited the best results for the generic data and was used for this study.

WIDAR: We chose 3 users for personalization since these were the only users whose data was collected in both rooms. Since the number of users in WIDAR is very small, the exclusion of all the 3 users for training the generic model would have resulted in substandard models. So, For each user, we generated different generic models by using data from the other 16 users with a 14/2 person disjoint random split for the train and validation set. Our classification target was the 6 gesture classes: 0,1,2,3,5 and 8, corresponding to push, sweep, clap, slide, draw a circle, and draw zigzag, respectively, as evaluated in the original work [94].

Model: The model used for WIDAR follows the LeNet architecture [94], which contains three 2D convolutional layers followed by two linear layers. Each of these layers, except the final classification layer, is followed by a ReLU activation layer.

ExtraSensory: We chose 5 users for personalization, and the generic model is trained on 42 users, with 10 users being left out for person-disjoint validation. The two target classes are walking and sitting.

Model: The model follows a CNN-GRU-based architecture used in HAR literature [23, 26, 69, 93]. The model consists of three batch-normalized 1D convolution layers followed by a linear layer that feeds into a batch-normalized recursive (GRU) layer and two linear layers to generate embeddings. For the classification head, two linear layers were used.

Stress Sensing Dataset: For this binary task, three users with data across all contexts were selected for personalization. The generic model was trained on data from 21 users, with six additional users for disjoint validation and test sets.

Model: The model uses a simple multi-layer-perceptron (MLP) architecture [16, 18, 89] consisting of 3 linear layers with hidden size of 128.

6.2 Metrics for evaluation

To establish the efficacy of **CRoP**, we quantify the extent of *personalization* and *generalization* achieved through the presented approach. Personalization is gauged by comparing our model's $\mathcal{M}_\theta^{P_i^a}$ accuracy relative to the generic model \mathcal{M}_θ^G , while for generalization, we assess the accuracy of our model $\mathcal{M}_\theta^{P_i^a}$ against *conventionally-finetuned* personalized models $\mathcal{M}_\theta^{C_i^a}$.

Taori et al. [76] argued that directly comparing model accuracies under distribution shifts is not ideal. They introduced ‘effective robustness,’ a metric that assesses performance relative to an accuracy baseline. Since we aim to compare our models against two baselines – the generic and conventionally finetuned models – we adopt the ‘effective robustness metric’ and introduce two specific metrics for our comparison, detailed below. Both of these metrics consider classification accuracy in the available C_a and unseen C_u contexts.

If $\mathcal{A}(\mathcal{M}, \mathcal{D})$ represents the classification accuracy of the model \mathcal{M} for dataset \mathcal{D} and n is the number of users selected for personalization, the metrics of evaluations can be described as follows :

- (1) Personalization (Δ_P): It is defined as the sum of the difference between the accuracy of $\mathcal{M}_\theta^{P_i^a}$ and \mathcal{M}_θ^G over all the contexts averaged over all users

$$\Delta_P = \frac{1}{n} \sum_{\mathcal{U}_i} \sum_{C \in \{C_a, C_u\}} (\mathcal{A}(\mathcal{M}_\theta^{P_i^a}, C) - \mathcal{A}(\mathcal{M}_\theta^G, C))$$

- (2) Generalization (Δ_G): It is defined as the sum of the difference between the accuracy of $\mathcal{M}_\theta^{P_i^a}$ and $\mathcal{M}_\theta^{C_i^a}$ over all the contexts averaged over all users.

$$\Delta_G = \frac{1}{n} \sum_{\mathcal{U}_i} \sum_{C \in \{C_a, C_u\}} (\mathcal{A}(\mathcal{M}_\theta^{P_i^a}, C) - \mathcal{A}(\mathcal{M}_\theta^{C_i^a}, C))$$

In summary, the metric Δ_P suggests how well the model $\mathcal{M}_\theta^{P_i^a}$ performs as compared to the generic model \mathcal{M}_θ^G . Since the generic model has not learned the person-specific patterns. This metric quantifies **CRoP**’s ability to learn person-specific patterns. On the other hand, conventionally finetuned models $\mathcal{M}_\theta^{C_i^a}$ may learn person-specific patterns and forget the generic information of different contexts. Thus, the metric Δ_G quantifies **CRoP**’s ability to retain generic information.

All the results in this section are computed as an average of accuracy obtained for three random seeds.

6.3 Comparison with State-of-the-art

To demonstrate the efficacy of **CRoP** in achieving personalization Δ_P while maintaining generalization Δ_G , we compare **CRoP** with 5 state-of-the-art approaches SHOT [43], PackNet [50], Piggyback [51], CoTTA [88], and PTN [10].

Table 4 compares the performance of **CRoP** with aforementioned baseline approaches. The values for Δ_P and Δ_G are computed as average over all the participants used for personalization for each dataset. The detailed results for participant-specific evaluations for each dataset are provided in Appendix B and Appendix B.3 shows the errors bars for our approach.

Table 4 shows that **CRoP** significantly outperforms all state-of-the-art (SOTA) methods. On average, the personalization benefits Δ_P achieved by SHOT, PackNet, Piggyback and CoTTA are 2.16, 26.05, 18.01, 9.95, and 4.13 percent points, respectively, while **CRoP** can achieve 35.23 percent points. However, while comparing Δ_G , one can observe that personalized training using SHOT, PackNet, Piggyback and CoTTA harms generalizability by -25.73, -1.39, -9.43, -17.49 and -23.44 percent points respectively. On the other hand, **CRoP** shows an average generalization benefit of 7.78.

	Approach	SHOT		Packnet		Piggyback		CoTTA		PTN		CRoP	
Dataset	Scenrio	Δ_P	Δ_G	Δ_P	Δ_G								
PERCEPT-R	Scenario 1	-3.11	-5.62	0.10	-2.41	-25.31	-27.83	-45.06	-47.58	-1.16	-3.68	5.08	2.57
Stress Sensing Single context Change	Scenario 1	-8.19	-62.16	54.70	0.70	43.89	-10.12	21.93	-32.07	1.23	-52.76	67.81	13.81
	Scenario 2	8.90	-63.27	75.80	3.64	66.22	-5.94	51.47	-20.69	21.76	-50.40	85.25	13.08
Stress Sensing Double context Change	Scenario 1	-0.49	-47.24	52.46	10.08	32.40	-9.97	30.59	-11.78	6.40	-35.98	54.38	12.00
	Scenario 2	3.57	-45.49	41.68	-7.36	42.76	-6.25	33.85	-15.19	12.30	-36.74	59.21	10.15
WIDAR	Scenario 1	1.67	-0.48	-0.24	-2.37	0.84	-1.28	-1.05	-3.18	-1.99	-4.37	8.56	6.43
	Scenario 2	1.28	-0.03	-3.55	-5.16	-8.97	-10.57	1.81	0.21	0.00	-2.85	5.90	4.30
ExtraSensory	Scenario 1	7.63	-10.31	12.19	-5.76	5.03	-12.91	-0.6	-18.54	1.69	-16.72	17.49	-0.46
	Scenario 2	8.17	2.99	1.33	-3.85	5.22	0.04	-3.43	-8.62	-3.02	-7.47	13.52	8.17

Table 4. Comparison of CRoP with baseline approaches under the metrics of Personalization (Δ_P) and Generalization (Δ_G).

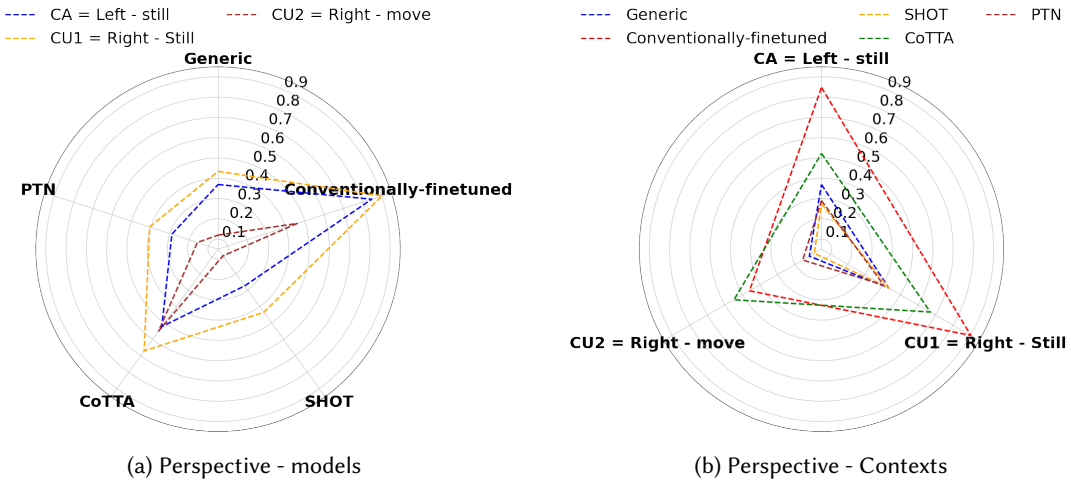


Fig. 3. Detailed results for Stress sensing dataset User 3 under Scenario 1 using F1 score as the evaluation metric

Notably, domain adaptation and continual learning methods, such as SHOT, Packnet, Piggyback, CoTTA, and PTN, leverage data from new contexts to adapt models while preserving knowledge from previous contexts or tasks. However, the problem addressed in this work requires the model to perform reasonably well in a completely unseen context, for which no data—labeled or unlabeled—is available during training. As a result, all baseline approaches struggle significantly in this scenario. Since the metrics in Section 6.2 evaluate performance across both available and unseen contexts, the substantial performance drop in the unseen context negatively impacts overall results. Furthermore, the unsupervised approaches SHOT, CoTTA, and PTN achieved lower Δ_P and Δ_G than supervised approaches Packnet, Piggyback, and CRoP, which is in line with literature [82].

The following discusses notable patterns observed in this section’s evaluations in Table 4, insights into the characteristics of static personalization across various human-sensing applications.

6.3.1 For stress-sensing dataset, all the unsupervised approaches show better performance on double context change than the single-context change. For Scenario 1, C_a contains samples of data collected using the left hand while staying still. For C_u^1 (single context change), the hand changes to the right while staying still, but in C_u^2 (double context change), both hand and motion status changes. Since C_u^2 incurs greater shift in context than C_u^1 , one can expect that a model trained on C_a will show similar or worse results for C_u^2 as compared to C_u^1 . However, unsupervised approaches—SHOT, CoTTA, and PTN—exhibit higher Δ_P and Δ_G values under C_u^2 than C_u^1 .

User-specific results, however, indicate that models actually perform worse on C_u^2 . Figure 3(a) shows detailed results in terms of F1 score for User 3 for generic model \mathcal{M}_θ^G , conventionally-finetuned model $\mathcal{M}_\theta^{P^a}$, and models generated using unsupervised approaches: SHOT, CoTTA and PTN under Scenario 1. As expected, all models perform worse with the double context change C_u^2 (CU2 = Right-move) compared to the single context change C_u^1 (CU1 = Right-still). Despite this, the Δ_P and Δ_G values suggest otherwise, explained as follows:

First, consider the Δ_P results, with the generic model as the accuracy baseline. Figure 3(b) shows that the generic model's F1 score drops significantly with the double context change C_u^2 compared to the single context change, C_u^1 , depicted on the blue lines. Although the performance benefits using the three approaches are almost similar in both unseen contexts, the difference in the performance as compared to the generic model is higher for double context change, thus resulting in higher Δ_P . Similarly, for Δ_G , with the conventionally finetuned model as the baseline, the best results are seen in the available context, C_a (Left-still). Its performance is only slightly affected by the single context change but drops significantly in C_u^2 due to movement during data collection, resulting in a higher Δ_G for the double context change.

Similar patterns were observed in other users, indicating that the poor performance of \mathcal{M}_θ^G and $\mathcal{M}_\theta^{P^a}$ during double context change drives the higher Δ_P and Δ_G values, giving an illusion of better results for double context change scenarios.

6.3.2 Significant performance drop for PERCEPT-R using SOTA approaches. For the Percept-R dataset, personalization applied to the 16 participants reveals that not all participants benefit equally. In some cases, the global models already perform well, leaving little to no room for improvement through personalization. In such cases, performance can even drop due to overfitting on the available context data. Our approach mitigates this by selecting the best model based on the highest validation accuracy from the available context, thus avoiding overfitting. Furthermore, CRoP introduces a trainable regularization coefficient during the initial finetuning phase, which penalizes model parameters while minimizing classification error (Algorithm 1 line 2 - trainable parameter α). This enables the maximal removal of less important weights during the ToleratedPrune step without impacting performance in the available context (Algorithm 1 line 3). Additionally, we found that finetuning after the model mixing step was often unnecessary, as the mixed model typically emerged as the best choice (Algorithm 1 line 5). In contrast, the baseline approaches lack these constraints, leading to performance degradation in both the available and unseen contexts, negatively affecting the overall results.

6.3.3 Inferior generic model performance leads to higher gain in personalization. For ExtraSensory and Stress-sensing datasets, certain users experience sub-optimal performance with the generic model \mathcal{M}_θ^G and the personalized finetuning helped not only in available context but also in the unseen contexts. For instance, the generic model showed suboptimal performance for certain users such as user '80' for ExtraSensory dataset under Scenario 1 and user '3' for Stress-sensing dataset. Such users show higher benefit even in the unseen context when personalized using available context data, highlighting the importance of user-specific patterns. The details explanation of these results are provided in Appendix B.

6.3.4 Significant Performance gains for the stress-sensing dataset for all approaches. Psychophysiological stress response is inherently heterogeneous in inter- and intra-user scenarios [54], leading to subpar performance of the generic model without personalization. As discussed in Section 6.3.3, subpar performance of generic models results in higher gain during personalization. This is evident from the significantly high Δ_P values achieved by most approaches for the stress-sensing dataset in Table 4.

These evaluations confirm that models personalized with CRoP exhibit higher generalizability to unseen contexts, making them more intra-user robust.

7 EMPIRICAL JUSTIFICATION FOR CROP

This section empirically justifies and discusses how the use of different components of **CRoP** helps in incorporating personalization (Δ_P) and generalization (Δ_G).

7.1 How different steps of **CRoP** facilitate generalizability

This section empirically discusses how each step of **CRoP** (Algorithm 1) facilitates intra-user generalizability, signifying similarity in the model's behavior towards available C_a (available during personalization finetuning) and unseen contexts C_u .

Shi et al. [70] introduced the use of gradient inner product (GIP) to estimate the similarity between a model's behavior across different domains. If G_i and G_j represent the gradient incurred by the model for Domains D_i and D_j , then the sign of the product $G_i * G_j$ represents whether the model treats two domains similarly or not. For instance, $G_i * G_j > 0$ signifies that the gradient for both domains has the same direction. We used GIP to quantify generalization. *A higher GIP value for a personalized model across available (C_a) and unseen contexts (C_u) indicates more similar behavior toward both domains, indicating higher intra-user generalizability.* GIP is measured as: $\| \sum_i G_i \|^2 - \sum_i \|G_i\|^2$.

Figure 4 shows that fine-tuning the generic model (Algorithm 1 – Step 2) on Context C_a , optimizes the model for this context, leading to a negative GIP, indicating a greater discrepancy between two contexts. Since model pruning results in generalization [34], an increase in GIP value can be observed in the pruned model (Step 3).

On further analysis, we found that the model complementary to the pruned model (that is, the parameters that were removed) also contributed towards inter-context behavior discrepancy (negative GIP value). However, the same parameters in the generic model (that are replaced in Step 4) formed a more generalizable set of weights, i.e., $GIP \geq 0$. Thus, the model mixing step (Step 4) introduces further generalizability ($GIP \geq 0$) in the personalized model.

Finally, as discussed in Section 5.2 and following Section 7.2, the objective of the final finetuning step is to recover the performance loss, and it doesn't aim to enhance generalizability further, as also shown in Figure 4.

7.2 Justification for the requirement of final finetuning step (Algorithm 1 Line 5) for some users

In Section 5.2, we discussed that the *Mixed Model* from Algorithm 1 Line 4 suffers accuracy loss due to altered activation paths, as it combines weights from the generic and personalized stages. To illustrate, we compare the performance and activation maps of the model states at step 2 ($\mathcal{M}^{P_i^a} \theta'$) and the *Mixed Model* ($\mathcal{M}^{P_i^a} \theta''$).

Table 5 shows that the *Mixed Model* $\mathcal{M}^{P_i^a} \theta''$ does show an average improvement of 14.43% in inference accuracy for the unseen context C_u , due to retainment of generic model weights; however, there is significant loss in the available context C_a as compared to

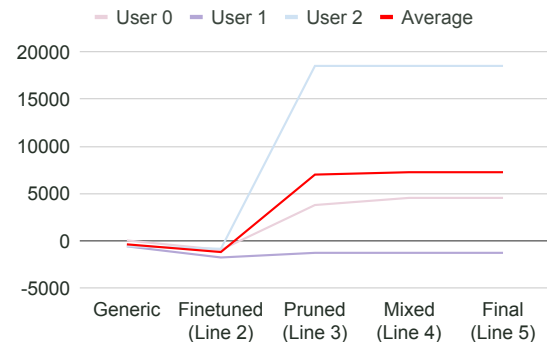


Fig. 4. Variation of GIP at different stages of **CRoP** signified by the lines in Algorithm 1

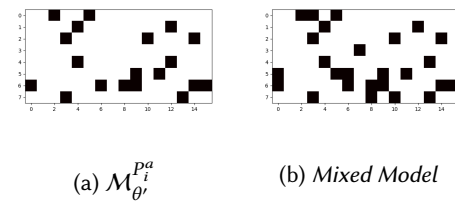


Fig. 5. Activation maps in C_a for Scenario 1

Model	$\mathcal{M}_{\theta'}^{P_i^a}$		$\mathcal{M}_{\theta''}^{P_i^a}$		$\mathcal{A}(\mathcal{M}_{\theta''}^{P_i^a}, C) - \mathcal{A}(\mathcal{M}_{\theta'}^{P_i^a}, C)$		$\mathcal{M}_{\theta}^{P_i^a}$		$\mathcal{A}(\mathcal{M}_{\theta}^{P_i^a}, C) - \mathcal{A}(\mathcal{M}_{\theta'}^{P_i^a}, C)$	
User	C_a	C_u	C_a	C_u	C_a	C_u	C_a	C_u	C_a	C_u
0	87.06	65.02	70.93	74.64	-16.13	+9.62	83.67	69.53	-3.39	+4.51
1	89.38	44.38	74.23	72.70	-15.15	+28.32	86.41	54.45	-2.97	+10.07
2	71.88	64.45	60.09	69.79	-11.79	+5.34	77.02	62.63	+5.14	-1.82
Average					-14.36	+14.43			-0.41	+4.25

Table 5. Performance Comparison of model states after initial finetuning (Algorithm 1 line 2), model mixing (Algorithm 1 line 4) and final finetuning (Algorithm 1 line 5) for WIDAR dataset under Scenario 1

the finetuned model $\mathcal{M}_{\theta'}^{P_i^a}$. We attribute this loss to both pruning-induced information loss and inconsistent changes in activation paths during model mixing. Figure 5 shows the change in the activation map for a sample from context C_a , which was correctly classifier by $\mathcal{M}_{\theta'}^{P_i^a}$; however, it got misclassified after the model mixing step. Significant differences in activation maps can be observed for this sample. This highlights the need for finetuning to recover lost information and restore consistent activation paths.

Table 5 further shows that the final finetuning step indeed helps recover the loss in the available context C_a . Although this may slightly reduce accuracy in the unseen context due to overwriting some generic patterns, it provides an average improvement of 4.25 percentage points in the unseen context C_u as compared to the model achieved after first finetuning (Algorithm 1 Line 2). This shows that the final finetuning is necessary for some users to regain performance lost in available context C_a .

8 DETAILS OF ABLATION STUDY

This section presents evaluations showing the effectiveness of the design choices of CRoP, focusing on the WIDAR dataset in Scenario 1. Figure 6 compares the current design choices with alternative options available in the literature. The comparison is done for each of the three users chosen for personalization under both available C_a and unseen C_u contexts. The metric used for this comparison is the inference accuracy. Similar patterns were observed in other scenarios and datasets.

8.1 Pruning mechanism

CRoP uses one-shot magnitude-based pruning (*MP*) [48, 96] to remove the lowest-magnitude model parameters in the ToleratedPrune module (Algorithm 1, Line 3). Various other pruning methods exist, most relevant ones being: Gradient-Based Pruning (*GP*) [46], pruning top-magnitude weights instead of lower ones (*MP* – *T*) [5], and iterative pruning (*MP* – *I*) [56] [30]. A comparative discussion of these methods is provided below.

Magnitude-based (*MP*) vs. Gradient-based Pruning (*GP*): Liu et al. [46] introduced gradient-based pruning (*GP*), which assigns importance to model parameters (i.e., kernels or nodes) based on the ℓ_1 norm of gradients (computed from the training set data) and prunes the least important ones. In literature (e.g., [38]), the approach has been shown to work on models trained and tested on the data having independent and identical distribution (IID). However, in this work, data from contexts C_a and C_u follow different distributions. Since, according to the problem setup, only C_a data is accessible, using *GP* in CRoP leads to overfitting on C_a and poor performance on unseen contexts C_u . In contrast, *MP* selects important parameters based solely on weight magnitude, making it more robust and resulting in better performance on C_u . As shown in Figures 6(a), *GP* performs well on C_a but consistently underperforms compared to *MP* on C_u across all three users.

Top prune (*MP* – *T*) vs. lower prune (*MP*): CRoP’s conventional magnitude-based pruning (*MP*) removes a percentage of the lowest-magnitude weights, which typically have minimal impact on model inference [48, 96].

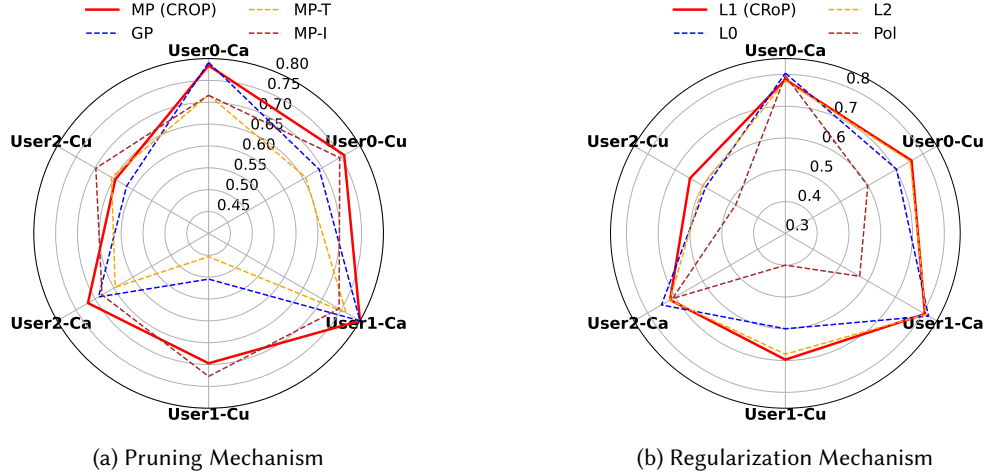


Fig. 6. Ablation study exploring different alternatives for (a) pruning and (b) regularization mechanisms using inference accuracy as the metric of evaluation

However, Bartoldson et al. [5] suggests that pruning the top weights and retraining them ($MP - T$) can improve generalization by creating flatter loss landscapes. Although $MP - T$ yields models that generalize better than traditional personalized models, Figure 6(a) shows that it performs significantly inferior to **CRoP** for all users in both contexts. This is because **CRoP** aims to isolate a user-specific sub-network that performs well in the available context C_a , rather than finding a generic sub-network. Pruning top weights removes user-specific information learned in step 2 of the Algorithm 1, which slightly improves performance in unseen context C_u but significantly degrades performance in context C_a . Moreover, since the removed top weights are important for C_a , the final finetuning stage (step 5 of the Algorithm 1) recaptures that information, overwriting the generic information, nullifying the approach’s effect.

One shot (MP) vs Iterative approach ($MP - I$) The presented approach, i.e., MP , uses a one-shot approach where the initially finetuned model undergoes one pass of pruning, mixing, and finetuning. However, we compared it with an iterative variation as well. To implement the iterative approach, $MP - I$, we allow the initially finetuned model to undergo multiple passes of pruning, mixing, and fine-tuning. As shown in Figure 6(a), $MP - I$ does not significantly improve model performance, yet it incurs high computational costs through repetition.

In the one-shot approach, the ‘ToleratedPrune’ module (Algorithm 1 line 3 and Algorithm 2) calculates the optimal pruning amount by removing the maximum parameters without exceeding the accuracy loss threshold τ for context C_a . In the iterative approach, we gradually reach the same pruning amount by removing small fractions of parameters for each cycle. These parameters are replaced by weights from the generic model, but since the finetuning loss function resembles the initial one, it drives those weights to lower magnitudes, causing them to be pruned again in the next cycle. This repeats until the target pruning amount is reached, effectively pruning a similar set of weights as the one-shot method but in smaller steps.

8.2 Regularization Mechanisms

CRoP uses regularization to push model parameters toward zero, making pruning easier in later steps. Weight penalty-based regularization methods apply different norms to the model’s weights, such as ℓ_0 , ℓ_1 , ℓ_2 , and polarization. The ℓ_1 norm is particularly effective because it not only reduces model parameters but also makes

Dataset	Platform	Train (s)	RSS (MBs)	Train Usage (%)
PERCEPT-R	AMD Ryzen 9 5950X 16-Core Processor	15.18	2787.36	24.99
	Apple M1	102.39	352	0.58
	NVIDIA RTX A6000	1.94	1132.61	20
	AMD Ryzen 9 7950X 16-Core Processor	14.22	830.97	24.9
	NVIDIA GeForce RTX 4090	1.54	1279.2	36
Stress-Sensing	AMD Ryzen 9 5950X 16-Core Processor	6.95	1469.59	24.9
	Apple M1	11.71	77	0.85
	NVIDIA RTX A6000	8.49	1071.14	7
	AMD Ryzen 9 7950X 16-Core Processor	3.13	633.27	25
	NVIDIA GeForce RTX 4090	4.31	1249.79	14

Table 6. Resource requirement for one time training using CRoP

the least significant parameters to zero. This property also makes ℓ_1 useful for feature selection [27]. Figure 6(b) compares all these possible regularization choices. We observed that among ℓ_0 , ℓ_1 , ℓ_2 and polarization [97], using ℓ_1 regularization is most effective in the unseen context. This is because, by forcing the least important parameter weights to zero, it allows maximum pruning with ‘ToleratedPrune,’ helping to recover as much generic information as possible.

8.3 Full finetune vs. partial finetune

In order to keep the zeroed-out parameters as zero, conventional pruning approaches finetune only the weights that are retained during the pruning phase. However, in the presented approach, the zeroed-out weights are replaced by corresponding weights from the generic model. Thus, there are no zero parameters. So, the presented approach finetunes all the parameters. We still evaluated both finetuning approaches and observed that there is no significant difference between the two approaches.

9 RUN-TIME ANALYSIS

CRoP is a static personalization approach that requires one-time on-device training of the generic model during personalization. We performed run-time evaluations to assess the viability of the CRoP framework across five different deployment platforms: AMD Ryzen 9 5950X 16-Core Processor, AMD Ryzen 9 7950X 16-Core Processor, Apple M1, NVIDIA RTX A6000 and NVIDIA GeForce RTX 4090. Table 6 shows the resources required in the training phase in terms of training time (s), process memory (MBs), and resource, i.e., GPU/CPU utilization (%) for two health-related datasets: PERCEPT-R and Stress-Sensing. According to our evaluation, except for the scalable device, Apple M1, the training time is a couple of seconds, and resource requirements are minimal. Even on scalable devices like Apple M1, computation time remains efficient, with only a slight increase, typically adding at most a few minutes. Since this is a one-time process, CRoP is efficient compared to continuous learning methods that require repeated adaptation. Particularly, this makes CRoP practical for critical applications, such as clinical settings, where it incurs only a brief, one-time computation overhead during enrollment.

10 LIMITATIONS AND FUTURE DIRECTION

Some limitations and future research are discussed below:

- (1) The paper performed a limited evaluation on pruning paradigms through ablation studies as it was not the primary focus of the study. Section 8 on ablation study justifies CRoP’s design choice but does not establish any particular paradigm’s superiority in unseen contexts.

- (2) As the approach relies on using a pre-trained off-the-shelf model as an input, the quality of this model can impact the performance of the final personalized models. As discussed in Section 6.3.3, users with suboptimal performance of the generic model show higher gain through personalization. On the other hand, for certain participants in the PERCEPT-R dataset, a high-performing model leaves minimal room for improvement through personalization.
- (3) We restrict our study to the models benchmarked and deployed for datasets used in this work without accounting for model variability. However, the different model architectures employed across all the datasets incorporate a range of layers such as convolutional, linear, BiLSTM, and GRU, which introduces some variability.
- (4) Some evaluation results, for instance, Table 4 evaluations are shown as average. However, the metrics Δ_P and Δ_G are calculated individually for each person. This is because models personalized for one user cannot be applied to other users in real-world situations. Consequently, we focus our evaluations on intra-user generalizability, excluding discussion for inter-user or inter-dataset generalizability.

11 BROADER IMPACT

This paper addresses a critical research gap, enhancing the practical utility of human-sensing solutions in real-world applications, particularly in automated healthcare. Next-generation healthcare systems, which employ neural networks for tasks ranging from daily activity detection [73, 78] to safety-critical conditions like atrial fibrillation [11], benefit from personalization due to the heterogeneity in health sensing data [33, 67]. **CRoP** offers several advantages:

- (1) Eliminating the Generic Model Training: **CRoP** leverages off-the-shelf pre-trained models, eliminating the need for training generic models. It is especially valuable in clinical settings where privacy concerns restrict data sharing for training purposes [49]. This increases the feasibility of deploying personalized models in healthcare.
- (2) No privacy concerns: **CRoP** operates on local devices, eliminating the need for transferring potentially sensitive information to a central server. To demonstrate scalability on local devices, the resource consumption for **CRoP** personalization on 5 devices is shown in Section 9.
- (3) Flexibility to use any model architectures: As model pruning has proven applicable to various model architectures, **CRoP** is not restricted to any model architecture constraints, ensuring wide-ranging applicability.

12 CONCLUSION

This study introduces **CRoP**, a novel static personalization approach generating context-wise intra-user robust models from limited context data. Using pruning in a novel way to balance personalization and generalization, empirical analysis on four human-sensing datasets shows **CRoP** models exhibit an average increase of 35.23% in *personalization* compared to generic models and 7.78% in generalization compared to *conventionally-finetuned* personalized models. **CRoP** utilizes off-the-shelf models, reducing training effort and addressing privacy concerns. With practical benefits and quantitative performance enhancements, **CRoP** facilitates reliable real-world deployment for AI-based human-sensing applications like healthcare.

REFERENCES

- [1] Farhad Ahamed and Farnaz Farid. Applying internet of things and machine-learning for personalized healthcare: Issues and challenges. In *2018 International Conference on Machine Learning and Data Engineering (iCMLDE)*, pages 19–21. IEEE, 2018.
- [2] Apple. Workout types on apple watch. <https://support.apple.com/en-us/HT207934>, 2023.
- [3] Martin Arjovsky, Léon Bottou, Ishaaan Gulrajani, and David Lopez-Paz. Invariant risk minimization, 2020. URL <https://arxiv.org/abs/1907.02893>.

- [4] Ayo Awobajo. 3 tips to make google assistant your own. <https://blog.google/products/assistant/how-to-personalize-google-assistant/>, 2023.
- [5] Brian R. Bartoldson, Ari S. Morcos, Adrian Barbu, and Gordon Erlebacher. The generalization-stability tradeoff in neural network pruning, 2020.
- [6] N. R. Benway and J. L. Preston. Artificial intelligence assisted speech therapy for /r/ using speech motor chaining and the percept engine: a single case experimental clinical trial with chainingai., 2023. URL <https://surface.syr.edu/etd/1703>.
- [7] Nina R Benway, Jonathan L Preston, Elaine Hitchcock, Yvan Rose, Asif Salekin, Wendy Liang, and Tara McAllister. Reproducible speech research with the artificial intelligence-ready PERCEPT corpora. *J. Speech Lang. Hear. Res.*, 66(6):1986–2009, June 2023.
- [8] Visar Berisha, Chelsea Krantsevich, P Richard Hahn, Shira Hahn, Gautam Dasarathy, Pavan Turaga, and Julie Liss. Digital medicine and the curse of dimensionality. *NPJ Digit. Med.*, 4(1):153, October 2021.
- [9] Mehdi Boukhechba, Anna N Baglione, and Laura E Barnes. Leveraging mobile sensing and machine learning for personalized mental health care. *Ergonomics in design*, 28(4):18–23, 2020.
- [10] David Burns, Philip Boyer, Colin Arrowsmith, and Cari Whyne. Personalized activity recognition with deep triplet embeddings. *Sensors*, 22(14), 2022. ISSN 1424-8220. doi: 10.3390/s22145222. URL <https://www.mdpi.com/1424-8220/22/14/5222>.
- [11] Jonah Comstock. Study: Apple watch paired with deep neural network detects atrial fibrillation with 97 percent accuracy, 2017.
- [12] Botos Csaba, Wenzuan Zhang, Matthias Müller, Ser-Nam Lim, Mohamed Elhoseiny, Philip Torr, and Adel Bibi. Label delay in online continual learning, 2024. URL <https://arxiv.org/abs/2312.00923>.
- [13] Zachary A. Daniels, Jun Hu, Michael Lomnitz, Phil Miller, Aswin Raghavan, Joe Zhang, Michael Piacentino, and David Zhang. Efficient model adaptation for continual learning at the edge, 2023.
- [14] Antonio D’Innocente and Barbara Caputo. Domain generalization with domain-specific aggregation modules. In Thomas Brox, Andrés Bruhn, and Mario Fritz, editors, *Pattern Recognition*, pages 187–198, Cham, 2019. Springer International Publishing. ISBN 978-3-030-12939-2.
- [15] Di Duan, Huanqi Yang, Guohao Lan, Tianxing Li, Xiaohua Jia, and Weitao Xu. Emgsense: A low-effort self-supervised domain adaptation framework for emg sensing. In *2023 IEEE International Conference on Pervasive Computing and Communications (PerCom)*, pages 160–170, 2023. doi: 10.1109/PERCOM56429.2023.10099164.
- [16] Maciej Dzieżyc, Martin Gjoreski, Przemysław Kazienko, Stanisław Saganowski, and Matjaž Gams. Can we ditch feature engineering? end-to-end deep learning for affect recognition from physiological sensor data. *Sensors*, 20(22):6535, 2020.
- [17] empetica. Real-time physiological signals: E4 eda/gsr sensor, 2015. URL <https://www.empatica.com/research/e4/>.
- [18] Eda Eren and Tuğba Selcen Navruz. Stress detection with deep learning using bvp and eda signals. In *2022 International Congress on Human-Computer Interaction, Optimization and Robotic Applications (HORA)*, pages 1–7. IEEE, 2022.
- [19] Enrico Fini, Victor G Turrisi da Costa, Xavier Alameda-Pineda, Elisa Ricci, Karteek Alahari, and Julien Mairal. Self-supervised models are continual learners. In *Proceedings of the IEEE/CVF Conference on Computer Vision and Pattern Recognition*, 2022.
- [20] US Food and Drug Administration. Proposed regulatory framework for modifications to artificial intelligence / machine learning-based software as a medical device. *US Food and Drug Administration: Silver Spring, MD, USA*, 63, 2019. doi: 10.1016/j.apergo.2017.04.011.
- [21] Yaroslav Ganin and Victor Lempitsky. Unsupervised domain adaptation by backpropagation. In *Proceedings of the 32nd International Conference on International Conference on Machine Learning - Volume 37*, ICML’15, page 1180–1189. JMLR.org, 2015.
- [22] Yaroslav Ganin, Evgeniya Ustinova, Hana Ajakan, Pascal Germain, Hugo Larochelle, François Laviolette, Mario Marchand, and Victor Lempitsky. Domain-adversarial training of neural networks. *J. Mach. Learn. Res.*, 17(1):2096–2030, January 2016. ISSN 1532-4435.
- [23] Taesik Gong, Yeonsu Kim, Jinwoo Shin, and Sung-Ju Lee. Metasense: few-shot adaptation to untrained conditions in deep mobile sensing. In *Proceedings of the 17th Conference on Embedded Networked Sensor Systems*, SenSys ’19, page 110–123, New York, NY, USA, 2019. Association for Computing Machinery. ISBN 9781450369503. doi: 10.1145/3356250.3360020. URL <https://doi.org/10.1145/3356250.3360020>.
- [24] Taesik Gong, Yewon Kim, Adiba Orzikulova, Yunxin Liu, Sung Ju Hwang, Jinwoo Shin, and Sung-Ju Lee. Dapper: Label-free performance estimation after personalization for heterogeneous mobile sensing. *Proceedings of the ACM on Interactive, Mobile, Wearable and Ubiquitous Technologies*, 7(2):1–27, 2023.
- [25] Sachin Goyal, Ananya Kumar, Sankalp Garg, Zico Kolter, and Aditi Raghunathan. Finetune like you pretrain: Improved finetuning of zero-shot vision models. In *Proceedings of the IEEE/CVF Conference on Computer Vision and Pattern Recognition (CVPR)*, pages 19338–19347, June 2023.
- [26] Yujiao Hao, Rong Zheng, and Boyu Wang. Invariant feature learning for sensor-based human activity recognition. *IEEE Transactions on Mobile Computing*, 21(11):4013–4024, 2022. doi: 10.1109/TMC.2021.3064252.
- [27] Amin Ul Haq, Jian Ping Li, Muhammad Hammad Memon, Jalaluddin khan, Asad Malik, Tanvir Ahmad, Amjad Ali, Shah Nazir, Ijaz Ahad, and Mohammad Shahid. Feature selection based on l1-norm support vector machine and effective recognition system for parkinson’s disease using voice recordings. *IEEE Access*, 7:37718–37734, 2019. doi: 10.1109/ACCESS.2019.2906350.
- [28] Md Yousuf Harun, Jhair Gallardo, Tyler L. Hayes, and Christopher Kanan. How Efficient Are Today’s Continual Learning Algorithms? . In *2023 IEEE/CVF Conference on Computer Vision and Pattern Recognition Workshops (CVPRW)*, pages 2431–2436, Los Alamitos, CA, USA, June 2023. IEEE Computer Society. doi: 10.1109/CVPRW59228.2023.00241. URL <https://doi.ieeecomputersociety.org/10.1109/CVPRW59228.2023.00241>.

CVPRW59228.2023.00241.

- [29] Tyler L. Hayes, Nathan D. Cahill, and Christopher Kanan. Memory efficient experience replay for streaming learning, 2019. URL <https://arxiv.org/abs/1809.05922>.
- [30] Torsten Hoefler, Dan Alistarh, Tal Ben-Nun, Nikoli Dryden, and Alexandra Peste. Sparsity in deep learning: Pruning and growth for efficient inference and training in neural networks. *J. Mach. Learn. Res.*, 22(1), jan 2021. ISSN 1532-4435.
- [31] Jin-Hyuk Hong, Julian Ramos, and Anind K. Dey. Toward personalized activity recognition systems with a semipopulation approach. *IEEE Transactions on Human-Machine Systems*, 46(1):101–112, 2016. doi: 10.1109/THMS.2015.2489688.
- [32] Andrea Iaboni, Sofija Spasojevic, Kristine Newman, Lori Schindel Martin, Angel Wang, Bing Ye, Alex Mihailidis, and Shehroz S Khan. Wearable multimodal sensors for the detection of behavioral and psychological symptoms of dementia using personalized machine learning models. *Alzheimer's & Dementia: Diagnosis, Assessment & Disease Monitoring*, 14(1):e12305, 2022.
- [33] Wenhui Ji, Jingyu Zhu, Wanxia Wu, Nanxiang Wang, Jiqing Wang, Jiansheng Wu, Qiong Wu, Xuewen Wang, Changmin Yu, Gaofeng Wei, et al. Wearable sweat biosensors refresh personalized health/medical diagnostics. *Research*, 2021.
- [34] Tian Jin, Michael Carbin, Daniel M. Roy, Jonathan Frankle, and Gintare Karolina Dziugaite. Pruning's effect on generalization through the lens of training and regularization. In Alice H. Oh, Alekh Agarwal, Danielle Belgrave, and Kyunghyun Cho, editors, *Advances in Neural Information Processing Systems*, 2022. URL <https://openreview.net/forum?id=OrcLKV9sKWp>.
- [35] James Kirkpatrick, Razvan Pascanu, Neil Rabinowitz, Joel Veness, Guillaume Desjardins, Andrei A. Rusu, Kieran Milan, John Quan, Tiago Ramalho, Agnieszka Grabska-Barwinska, Demis Hassabis, Claudia Clopath, Dharshan Kumaran, and Raia Hadsell. Overcoming catastrophic forgetting in neural networks. *Proceedings of the National Academy of Sciences*, 114(13):3521–3526, 2017. doi: 10.1073/pnas.1611835114. URL <https://www.pnas.org/doi/abs/10.1073/pnas.1611835114>.
- [36] Wouter M. Kouw and Marco Loog. An introduction to domain adaptation and transfer learning, 2019. URL <https://arxiv.org/abs/1812.11806>.
- [37] Daniel B Kowalsky, John R Rebula, Lauro V Ojeda, Peter G Adamczyk, and Arthur D Kuo. Human walking in the real world: Interactions between terrain type, gait parameters, and energy expenditure. *PLoS One*, 16(1):e0228682, January 2021.
- [38] Alex Krizhevsky and Geoffrey Hinton. Learning multiple layers of features from tiny images. Technical report, University of Toronto, Toronto, Ontario, 2009. URL <https://www.cs.toronto.edu/~kriz/learning-features-2009-TR.pdf>.
- [39] Bishal Lamichhane, Joanne Zhou, and Akane Sano. Psychotic relapse prediction in schizophrenia patients using a personalized mobile sensing-based supervised deep learning model. *IEEE Journal of Biomedical and Health Informatics*, 2023.
- [40] Barbara A Lewis, Lisa Freebairn, Jessica Tag, Allison A Ciesla, Sudha K Iyengar, Catherine M Stein, and H Gerry Taylor. Adolescent outcomes of children with early speech sound disorders with and without language impairment. *Am. J. Speech. Lang. Pathol.*, 24(2):150–163, May 2015.
- [41] Da Li, Yongxin Yang, Yi-Zhe Song, and Timothy M. Hospedales. Learning to generalize: meta-learning for domain generalization. In *Proceedings of the Thirty-Second AAAI Conference on Artificial Intelligence and Thirtieth Innovative Applications of Artificial Intelligence Conference and Eighth AAAI Symposium on Educational Advances in Artificial Intelligence, AAAI'18/IAAI'18/EAAI'18*. AAAI Press, 2018. ISBN 978-1-57735-800-8.
- [42] Jingjing Li, Erpeng Chen, Zhengming Ding, Lei Zhu, Ke Lu, and Heng Tao Shen. Maximum density divergence for domain adaptation. *IEEE Transactions on Pattern Analysis and Machine Intelligence*, 43(11):3918–3930, 2021. doi: 10.1109/TPAMI.2020.2991050.
- [43] Jian Liang, Dapeng Hu, and Jiashi Feng. Do we really need to access the source data? source hypothesis transfer for unsupervised domain adaptation. In *International Conference on Machine Learning (ICML)*, pages 6028–6039, 2020.
- [44] Hanbing Liu, Jingge Wang, Xuan Zhang, Ye Guo, and Yang Li. Enhancing continuous domain adaptation with multi-path transfer curriculum, 2024.
- [45] Xin Liu, Yuntao Wang, Sinan Xie, Xiaoyu Zhang, Zixian Ma, Daniel McDuff, and Shwetak Patel. Mobilephys: Personalized mobile camera-based contactless physiological sensing. *Proc. ACM Interact. Mob. Wearable Ubiquitous Technol.*, 6(1), mar 2022. doi: 10.1145/3517225. URL <https://doi.org/10.1145/3517225>.
- [46] Xue Liu, Weijie Xia, and Zhimiao Fan. A deep neural network pruning method based on gradient l1-norm. In *2020 IEEE 6th International Conference on Computer and Communications (ICCC)*, pages 2070–2074, 2020. doi: 10.1109/ICCC51575.2020.9345039.
- [47] Mingsheng Long, Jianmin Wang, Yue Cao, Jiaguang Sun, and Philip S. Yu. Deep learning of transferable representation for scalable domain adaptation. *IEEE Transactions on Knowledge and Data Engineering*, 28(8):2027–2040, 2016. doi: 10.1109/TKDE.2016.2554549.
- [48] Jian-Hao Luo, Jianxin Wu, and Weiyao Lin. Thinet: A filter level pruning method for deep neural network compression. In *ICCV*, pages 5058–5066, 2017.
- [49] Bradley Malin, Kenneth Goodman, et al. Between access and privacy: challenges in sharing health data. *Yearbook of medical informatics*, 27(01):055–059, 2018.
- [50] Arun Mallya and Svetlana Lazebnik. Packnet: Adding multiple tasks to a single network by iterative pruning. In *2018 IEEE/CVF Conference on Computer Vision and Pattern Recognition*, pages 7765–7773, 2018. doi: 10.1109/CVPR.2018.00810.
- [51] Arun Mallya, Dillon Davis, and Svetlana Lazebnik. Piggyback: Adapting a single network to multiple tasks by learning to mask weights. In Vittorio Ferrari, Martial Hebert, Cristian Sminchisescu, and Yair Weiss, editors, *Computer Vision – ECCV 2018*, pages 72–88, Cham,

2018. Springer International Publishing. ISBN 978-3-030-01225-0.

[52] K. Mayank. Bxd primer series: Lasso regression models, l1 regularization in general and comparison with l2 regularization, 2023. URL <https://www.linkedin.com/pulse/bxd-primer-series-lasso-regression-models-l1-general-comparison-k-/>.

[53] Lakmal Meegahapola, William Droz, Peter Kun, Amalia De Götzen, Chaitanya Nutakki, Shyam Diwakar, Salvador Ruiz Correa, Donglei Song, Hao Xu, and Miriam Bidoglio. Generalization and personalization of mobile sensing-based mood inference models: An analysis of college students in eight countries. *Proceedings of the ACM on Interactive, Mobile, Wearable and Ubiquitous Technologies*, 6(4):1–32, 2023.

[54] Sujay Nagaraj, Sarah Goodday, Thomas Hartvigsen, Adrien Boch, Kopal Garg, Sindhu Gowda, Luca Foschini, Marzyeh Ghassemi, Stephen Friend, and Anna Goldenberg. Dissecting the heterogeneity of “in the wild” stress from multimodal sensor data. *NPJ Digital Medicine*, 6(1):237, 2023.

[55] Laura Päeske, Tuuli Uudeberg, Hiie Hinrikus, Jaanus Lass, and Maie Bachmann. Correlation between electroencephalographic markers in the healthy brain. *Sci. Rep.*, 13(1):6307, April 2023.

[56] Michela Paganini and Jessica Forde. On iterative neural network pruning, reinitialization, and the similarity of masks, 2020.

[57] Wonil Park, Victor J. Lee, Byungmo Ku, and Hirofumi Tanaka. Effect of walking speed and placement position interactions in determining the accuracy of various newer pedometers. *Journal of Exercise Science & Fitness*, 12(1):31–37, 2014. ISSN 1728-869X. doi: <https://doi.org/10.1016/j.jesf.2014.01.003>. URL <https://www.sciencedirect.com/science/article/pii/S1728869X14000057>.

[58] David Phelan. Amazon admits listening to alexa conversations: Why it matters. <https://shorturl.at/fxN78>, 2019.

[59] Michael Potuck. How to reset your apple watch fitness calibration for more accurate workout and activity data. <https://9to5mac.com/2021/08/26/fix-apple-watch-workout-tracking-activity-tracking/>, 2021.

[60] A. Prabhu, H. Al Kader Hammoud, P. Dokania, P. S. Torr, S. Lim, B. Ghanem, and A. Bibi. Computationally budgeted continual learning: What does matter? In *2023 IEEE/CVF Conference on Computer Vision and Pattern Recognition (CVPR)*, pages 3698–3707, Los Alamitos, CA, USA, jun 2023. IEEE Computer Society. doi: 10.1109/CVPR52729.2023.00360. URL <https://doi.ieeecomputersociety.org/10.1109/CVPR52729.2023.00360>.

[61] Amy Rathbone, Simone Stumpf, Caroline Claisse, Elizabeth Sillence, Lynne Coventry, Richard D Brown, and Abigail C Durrant. People with long-term conditions sharing personal health data via digital health technologies: A scoping review to inform design. *PLOS Digit. Health*, 2(5):e0000264, May 2023.

[62] Boyu Ren, Emma G Balkind, Brianna Pastro, Elana S Israel, Diego A Pizzagalli, Habiballah Rahimi-Eichi, Justin T Baker, and Christian A Webb. Predicting states of elevated negative affect in adolescents from smartphone sensors: A novel personalized machine learning approach. *Psychological Medicine*, pages 1–9, 2022.

[63] Xavier Robert-Lachaine, Hakim Mecheri, Christian Larue, and Andre Plamondon. Effect of local magnetic field disturbances on inertial measurement units accuracy. *Applied Ergonomics*, 63:123–132, 09 2017. doi: 10.1016/j.apergo.2017.04.011.

[64] Sadiq Sani, Stewart Massie, Nirmalje Wiratunga, and Kay Cooper. Learning deep and shallow features for human activity recognition. In Gang Li, Yong Ge, Zili Zhang, Zhi Jin, and Michael Blumenstein, editors, *Knowledge Science, Engineering and Management*, pages 469–482, Cham, 2017. Springer International Publishing. ISBN 978-3-319-63558-3.

[65] Philip Schmidt, Attila Reiss, Robert Duerichen, Claus Marberger, and Kristof Van Laerhoven. Introducing wesad, a multimodal dataset for wearable stress and affect detection. In *Proceedings of the 20th ACM International Conference on Multimodal Interaction, ICMI ’18*, page 400–408, New York, NY, USA, 2018. Association for Computing Machinery. ISBN 9781450356923. doi: 10.1145/3242969.3242985. URL <https://doi.org/10.1145/3242969.3242985>.

[66] Florian Schroff, Dmitry Kalenichenko, and James Philbin. Facenet: A unified embedding for face recognition and clustering. *2015 IEEE Conference on Computer Vision and Pattern Recognition (CVPR)*, Jun 2015. doi: 10.1109/cvpr.2015.7298682. URL <http://dx.doi.org/10.1109/CVPR.2015.7298682>.

[67] Juliane R Sempionatto, Victor Ruiz-Valdepenas Montiel, Eva Vargas, Hazhir Teymourian, and Joseph Wang. Wearable and mobile sensors for personalized nutrition. *ACS sensors*, 6(5):1745–1760, 2021.

[68] Shiv Shankar, Vihari Piratla, Soumen Chakrabarti, Siddhartha Chaudhuri, Preethi Jyothi, and Sunita Sarawagi. Generalizing across domains via cross-gradient training. In *ICLR (Poster)*. OpenReview.net, 2018. URL <http://dblp.uni-trier.de/db/conf/iclr/iclr2018.html#ShankarPCCJS18>.

[69] Qiang Shen, Haotian Feng, Rui Song, Stefano Teso, Fausto Giunchiglia, and Hao Xu. Federated multi-task attention for cross-individual human activity recognition. In Lud De Raedt, editor, *Proceedings of the Thirty-First International Joint Conference on Artificial Intelligence, IJCAI-22*, pages 3423–3429. International Joint Conferences on Artificial Intelligence Organization, 7 2022. doi: 10.24963/ijcai.2022/475. URL <https://doi.org/10.24963/ijcai.2022/475>. Main Track.

[70] Yuge Shi, Jeffrey Seely, Philip H. S. Torr, N. Siddharth, Awni Hannun, Nicolas Usunier, and Gabriel Synnaeve. Gradient matching for domain generalization. 2021.

[71] Leslie N Smith. Cyclical learning rates for training neural networks. In *2017 IEEE winter conference on applications of computer vision (WACV)*, pages 464–472. IEEE, 2017.

[72] Gabriela M Stegmann, Shira Hahn, Julie Liss, Jeremy Shefner, Seward Rutkove, Kerisa Shelton, Cayla Jessica Duncan, and Visar Berisha. Early detection and tracking of bulbar changes in ALS via frequent and remote speech analysis. *NPJ Digit. Med.*, 3(1):132, October 2020.

[73] Allan Stisen, Henrik Blunck, Sourav Bhattacharya, Thor Siiger Prentow, Mikkel Baum Kjærgaard, Anind Dey, Tobias Sonne, and Mads Møller Jensen. Smart devices are different: Assessing and mitigating mobile sensing heterogeneities for activity recognition. In *Proceedings of the 13th ACM conference on embedded networked sensor systems*, pages 127–140, 2015.

[74] C. Tang, L. Qendro, D. Spathis, F. Kawsar, C. Mascolo, and A. Mathur. Kaizen: Practical self-supervised continual learning with continual fine-tuning. In *2024 IEEE/CVF Winter Conference on Applications of Computer Vision (WACV)*, pages 2829–2838, Los Alamitos, CA, USA, jan 2024. IEEE Computer Society. doi: 10.1109/WACV57701.2024.00282. URL <https://doi.ieee.org/10.1109/WACV57701.2024.00282>.

[75] Chi Ian Tang, Lorena Qendro, Dimitris Spathis, Fahim Kawsar, Akhil Mathur, and Cecilia Mascolo. Balancing continual learning and fine-tuning for human activity recognition. *ArXiv*, abs/2401.02255, 2024. URL <https://api.semanticscholar.org/CorpusID:266755926>.

[76] Rohan Taori, Achal Dave, Vaishaal Shankar, Nicholas Carlini, Benjamin Recht, and Ludwig Schmidt. Measuring robustness to natural distribution shifts in image classification. In *Proceedings of the 34th International Conference on Neural Information Processing Systems, NIPS '20*, Red Hook, NY, USA, 2020. Curran Associates Inc. ISBN 9781713829546.

[77] Siri Team. Hey siri: An on-device dnn-powered voice trigger for apple's personal assistant. <https://machinelearning.apple.com/research/heysiri>, 2017.

[78] Yunus Emre Ustev, Ozlem Durmaz Incel, and Cem Ersoy. User, device and orientation independent human activity recognition on mobile phones: Challenges and a proposal. In *Proceedings of the 2013 ACM conference on Pervasive and ubiquitous computing adjunct publication*, pages 1427–1436, 2013.

[79] Yonatan Vaizman, Katherine Ellis, and Gert Lanckriet. Recognizing detailed human context in the wild from smartphones and smartwatches. *IEEE Pervasive Computing*, 16(4):62–74, 2017. doi: 10.1109/MPRV.2017.3971131.

[80] Gido M. van de Ven and Andreas S. Tolias. Generative replay with feedback connections as a general strategy for continual learning, 2019. URL <https://arxiv.org/abs/1809.10635>.

[81] Gido M van de Ven, Hava T Siegelmann, and Andreas S Tolias. Brain-inspired replay for continual learning with artificial neural networks. *Nat. Commun.*, 11(1):4069, August 2020.

[82] C. Varma and Puja Prasad. Supervised and unsupervised machine learning approaches—a survey, 02 2023.

[83] Tanvi Verma, Liyuan Jin, Jun Zhou, Jia Huang, Mingrui Tan, Benjamin Chen Ming Choong, Ting Fang Tan, Fei Gao, Xinxing Xu, Daniel S. Ting, and Yong Liu. Privacy-preserving continual learning methods for medical image classification: a comparative analysis. *Frontiers in Medicine*, 10, 2023. ISSN 2296-858X. doi: 10.3389/fmed.2023.1227515. URL <https://www.frontiersin.org/journals/medicine/articles/10.3389/fmed.2023.1227515>.

[84] Riccardo Volpi, Hongseok Namkoong, Ozan Sener, John Duchi, Vittorio Murino, and Silvio Savarese. Generalizing to unseen domains via adversarial data augmentation. In *Proceedings of the 32nd International Conference on Neural Information Processing Systems, NIPS'18*, page 5339–5349, Red Hook, NY, USA, 2018. Curran Associates Inc.

[85] Chan Wang, Tianyi He, Hong Zhou, Zixuan Zhang, and Chengkuo Lee. Artificial intelligence enhanced sensors - enabling technologies to next-generation healthcare and biomedical platform. *Bioelectron. Med.*, 9(1):17, August 2023.

[86] Jindong Wang, Cuiling Lan, Chang Liu, Yidong Ouyang, Tao Qin, Wang Lu, Yiqiang Chen, Wenjun Zeng, and Philip S. Yu. Generalizing to unseen domains: A survey on domain generalization. *IEEE Transactions on Knowledge and Data Engineering*, 35(8):8052–8072, 2023. doi: 10.1109/TKDE.2022.3178128.

[87] Qin Wang, Olga Fink, Luc Van Gool, and Dengxin Dai. Continual test-time domain adaptation, 2022.

[88] Qin Wang, Olga Fink, Luc Van Gool, and Dengxin Dai. Continual test-time domain adaptation. In *Proceedings of Conference on Computer Vision and Pattern Recognition*, 2022.

[89] Zhiguang Wang, Weizhong Yan, and Tim Oates. Time series classification from scratch with deep neural networks: A strong baseline. In *2017 International joint conference on neural networks (IJCNN)*, pages 1578–1585. IEEE, 2017.

[90] Yanan Wu, Zhixiang Chi, Yang Wang, Konstantinos N. Plataniotis, and Songhe Feng. Test-time domain adaptation by learning domain-aware batch normalization, 2024.

[91] Yi Xiao, Harshit Sharma, Zhongyang Zhang, Dessa Bergen-Cico, Tauhidur Rahman, and Asif Salekin. Reading between the heat: Co-teaching body thermal signatures for non-intrusive stress detection. *Proc. ACM Interact. Mob. Wearable Ubiquitous Technol.*, 7(4), jan 2024. doi: 10.1145/3631441. URL <https://doi.org/10.1145/3631441>.

[92] Jianfei Yang, Xinyan Chen, Dazhuo Wang, Han Zou, Chris Xiaoxuan Lu, Sumei Sun, and Lihua Xie. Sensefi: A library and benchmark on deep-learning-empowered wifi human sensing, 2023.

[93] Shuochao Yao, Shaohan Hu, Yiran Zhao, Aston Zhang, and Tarek Abdelzaher. Deepsense: A unified deep learning framework for time-series mobile sensing data processing. In *Proceedings of the 26th International Conference on World Wide Web, WWW '17*, page 351–360, Republic and Canton of Geneva, CHE, 2017. International World Wide Web Conferences Steering Committee. ISBN 9781450349130. doi: 10.1145/3038912.3052577. URL <https://doi.org/10.1145/3038912.3052577>.

[94] Y. Zhang, Y. Zheng, K. Qian, G. Zhang, Y. Liu, C. Wu, and Z. Yang. Widar3.0: Zero-effort cross-domain gesture recognition with wi-fi. *IEEE Transactions on Pattern Analysis and Machine Intelligence*, 44(11):8671–8688, nov 2022. ISSN 1939-3539. doi: 10.1109/TPAMI.2021.3105387.

- [95] Kaiyang Zhou, Yongxin Yang, Timothy Hospedales, and Tao Xiang. Deep domain-adversarial image generation for domain generalisation. *Proceedings of the AAAI Conference on Artificial Intelligence*, 34:13025–13032, 04 2020. doi: 10.1609/aaai.v34i07.7003.
- [96] Michael Zhu and Suyog Gupta. To prune, or not to prune: exploring the efficacy of pruning for model compression, 2017.
- [97] Tao Zhuang, Zhixuan Zhang, Yuheng Huang, Xiaoyi Zeng, Kai Shuang, and Xiang Li. Neuron-level structured pruning using polarization regularizer. In H. Larochelle, M. Ranzato, R. Hadsell, M.F. Balcan, and H. Lin, editors, *Advances in Neural Information Processing Systems*, volume 33, pages 9865–9877. Curran Associates, Inc., 2020. URL https://proceedings.neurips.cc/paper_files/paper/2020/file/703957b6dd9e3a7980e040bee50ded65-Paper.pdf.

A ENSURING REPRODUCIBILITY

Depending on the distribution of the data, different accuracy measures have been used in the literature such as balanced accuracy, standard accuracy, or F1 score. To ensure consistency with the original baseline papers for each dataset [7, 91], we follow their evaluation metric. Detailed explanations and justifications are provided in Appendix A.1. To ensure reproducibility, we provide the hyperparameters used in both the general model training phase and the personalization phase in Appendix A.2. This includes learning rate, alpha, τ , epoch count, and other settings specific to each dataset. Additionally Appendix A.3 and Appendix A.4 provide details of the code and the compute resources, respectively.

A.1 Metrics for classification accuracy evaluation

We use accuracy to measure the performance of a model. However, the computation of this metric differs for the four datasets. The details of the metrics used for all the datasets are as follows:

- (1) PERCEPT-R: For this dataset, Benway et al. [7] utilized balanced accuracy for the binary classification task, and we employed the same metrics in our study.
- (2) WIDAR: We use a 6-class classification for gesture recognition, and the distribution of the data among these classes is nearly balanced. Thus, standard classification accuracy has been used for WIDAR.
- (3) ExtraSensory: The subset of the Extrasensory dataset used for this work aims for a binary classification for activity recognition. We observed that the data distribution was quite imbalanced among the two classes, and therefore, balanced classification accuracy was used for this dataset. Balanced accuracy is computed as the average of true positive rate and true negative rate.
- (4) Stress Sensing Dataset: For this binary classification problem, F1 score has been used as a performance metric as suggested by the original authors [91].

For simplicity, we use the term ‘accuracy’ to encompass all the metrics discussed above.

A.2 Hyperparameters

The approach uses several hyperparameters for generic model training and personalization. Table 7 and 8 show the hyperparameter values for generic and personalized model training, respectively. These values correspond to the best results obtained for the data belonging to the available context using a grid search. For training the generic model, in addition to the number of epochs, ‘Base Learning Rate’ and ‘Max Learning Rate’ (the arguments for CycleLR [71]) are the hyperparameters. For the personalized model, learning rate (fixed), α , τ , number of epochs for initial finetuning (Initial Epochs), and epochs for final finetuning (Final Epochs) are the hyperparameters. The range of these hyperparameters used for grid search during personalization is also mentioned in Table 8.

Additionally, we use $k = k' = 0.05$ for the *ToleratedPrune* module for PERCEPT-R, WIDAR, and ExtraSensory datasets, while for the Stress-sensing dataset, $k = 0.05$ and $k' = 0.01$ is being used. One may find different values to be suitable for other datasets and model architectures.

Hyperparameter	PERCEPT-R	WIDAR	ExtraSensory	Stress-sensing
Base Learning Rate	1e-5	1e-07	1.2e-08	5e-5
Max Learning Rate	1e-5	5e-06	7.5e-07	5e-5
Epochs	300	1000	150	1000

Table 7. Hyperparameters for generic Models

Hyperparameter	Range	PERCEPT-R	WIDAR	ExtraSensory	Stress Sensing
Learning Rate	1e-6 - 1e-1	1e-5	1e-6	1e-6	1e-5
α	1e-6 - 10	0.01	0.0001	0.5	0.0001
τ	0.01 - 0.25	0.05	0.2	0.01	0.01
Initial Epochs	100 - 1000	300	600	600	1000
Final Epochs	100 - 1000	300	600	1000	1000

Table 8. Hyperparameters for Personalized Models

A.3 Code

The code is provided at anonymous link arranged into dataset-specific folders. Each folder contains the pre-trained generic model, all the required modules, and the instructions to run the code. The seed values used for the evaluations are also provided in the shell files. The data partitioned into personalized and context-wise sets will be released upon publication.

A.4 Compute Resources

All the computations have been performed on NVIDIA Quadro RTX 5000 with 48 RT Cores and 16GB GDDR6 memory.

B DETAILED USER-SPECIFIC RESULTS

This section discusses the user-specific patterns. Appendix B.1 discusses detailed personalization (Δ_P) results while Appendix B.2 discusses generalization (Δ_G) results. Further, Appendix B.3 shows person-wise standard deviation values for generic \mathcal{M}_θ^G , conventionally finetuned $\mathcal{M}_\theta^{C_i^a}$ and **CRoP** $\mathcal{M}_\theta^{P_i^a}$ models.

B.1 Detailed discussion of Δ_P results

The personalized models obtained using **CRoP** exhibit higher classification accuracy than the generic models on the available context's data \mathcal{D}_i^a , showcasing the benefits of personalization. To demonstrate the existence of such improvement, Tables 9a- 9h and Table 11a compare the performance of generic model \mathcal{M}_θ^G and personalized models obtained using **CRoP** $\mathcal{M}_\theta^{P_i^a}$.

WIDAR: Tables 9a and 9b show that there is an average improvement of 25.25 and 11.88 percent points among three users for the available context C_a for Scenario 1 and Scenario 2, respectively. However, this benefit comes at the cost of a reduction in accuracy for the unseen context. There is an average reduction of 16.69 and 5.97 percent points for Scenario 1 and Scenario 2, respectively, for the unseen context C_u . Notably, the loss of accuracy in the unseen context is much lower as compared to the *conventionally-finetune* model as discussed in the Section 3 (Motivation).

ExtraSensory: Similar patterns could be observed for the Extrasensory dataset. Tables 9c and 9d show that there is an average increment of 16.40 and 18.37 percent points for the available context for Scenario 1 and

Scenario 2, respectively. Interestingly, the performance of the personalized model for Scenario 1 on unseen context C_u was not adversely impacted. This is attributed to the fact that the inertial sensing patterns of Bag and Pocket phone carrying modes capture the user's body movement, whereas the phone-in-hand movement patterns can be distinct. In Scenario 1, C_a comprises pocket and C_u comprises bag, meaning both available and unseen contexts encompass similar inertial patterns, leading to advantageous performance even in the unseen context. *This evaluation illustrates minimal intra-user generalizability loss on unseen contexts when both available and unseen contexts share similar user traits.* However, in Scenario 2, where only the hand belongs to the unseen context C_u , there is an average loss of 5.02 percentage points on the unseen context.

Stress Sensing: The physiological features used in this dataset vary significantly from one user to other. Thus, Tables 9e-9h show that the generic models do not perform well on personalized data. Personalized finetuning enables the model to learn person-specific patterns, allowing the model's performance to improve not only in the available context but also in the unseen context. This results in average personalization benefit (Δ_P) of 67.81 and 85.25 for Scenario 1 and Scenario 2, respectively. It is important to note that for each Scenario, only one model is trained for the available context and tested for two different unseen contexts. Moreover, double context change (Tables 9g and 9h) shows lower personalization benefit as compared to single context change (Tables 9e and 9f).

PERCEPT-R: In this dataset, the heterogeneity of features among individuals is reflected through the difference in prediction accuracy of the generic model. It can be observed in Table 11a that for some individuals, the generic model exhibits over 90% accuracy on the available context data, while for others, the generic model's accuracy drops to around 60%. This results in significant variability over gains in available and unseen contexts. Overall, CRoP yields an average personalization gain of 5.09%.

On average over all the datasets, a personalization benefit (Δ_P) of 35.23 percent points are seen as compared to the generic models across the four datasets under both scenarios.

These evaluations establish that the personalized models obtained using CRoP demonstrate improved performance over the available context data than the generic models and exhibit personalization.

B.2 Detailed discussion of Δ_G results

The personalized models obtained using CRoP ($\mathcal{M}_\theta^{P_i^a}$) are expected to have higher accuracy on unseen context C_u than the *conventionally-finetune* personalized models ($\mathcal{M}_\theta^{C_i^a}$) as discussed in Section 3. This section assesses whether the results align with these expectations.

WIDAR: Tables 10a and 10b demonstrate that the personalized models $\mathcal{M}_\theta^{P_i^a}$ exhibit an average increment of 8.01 and 2.85 percent points in the unseen context for Scenario 1 and Scenario 2, respectively. However, an average loss of 1.57 and an average gain of 1.44 percent points in C'_a 's accuracy could be observed for Scenario 1 and Scenario 2, respectively.

Extrasensory: Similar patterns could be observed for the ExtraSensory dataset where the average accuracy on the unseen context improved by 4.97 and 12.61 percentage points for Scenario 1 and Scenario 2 as shown in Tables 9c and 10d, respectively. As expected, there is a loss of 5.43 and 4.44 percent points in the available contexts for Scenario 1 and Scenario 2, respectively.

Stress Sensing: As observed in Tables 9e-9h, personalized finetuning improves models performance on unseen context as well, we can claim that there is some person-specific traits which are common in available and unseen context. While comparing our final models with *conventionally-finetuned* models (Tables 10e-10h), performance boost in both available and unseen context could be observed. This can be attributed to the generalization improvement benefits of model pruning [34]. This results in average generalization benefit (Δ_G) of 13.81 and

(a) Scenario 1 for WIDAR dataset						(b) Scenario 2 for WIDAR dataset							
Model	\mathcal{M}_θ^G		$\mathcal{M}_\theta^{P_i}$		$\mathcal{A}(\mathcal{M}_\theta^{P_i}, C) - \mathcal{A}(\mathcal{M}_\theta^G, C)$		Model	\mathcal{M}_θ^G		$\mathcal{M}_\theta^{P_i}$		$\mathcal{A}(\mathcal{M}_\theta^{P_i}, C) - \mathcal{A}(\mathcal{M}_\theta^G, C)$	
User	C_a	C_u	C_a	C_u	C_a	C_u	User	C_a	C_u	C_a	C_u	C_a	C_u
0	63.90	77.09	83.67	69.53	+19.77	-7.56	0	73.28	61.80	82.59	58.38	+9.31	-2.43
1	61.80	79.78	86.41	54.45	+24.61	-25.33	1	73.18	59.58	92.44	47.90	+19.27	-11.67
2	45.63	79.81	77.02	62.63	+31.38	-17.18	2	80.45	46.13	87.5	42.31	+7.04	-3.81
Average					+25.25	-16.69	Average					+11.88	-5.97
Δ_P						+8.55	Δ_P						+5.90

(c) Scenario 1 for ExtraSensory dataset						(d) Scenario 2 for ExtraSensory dataset							
Model	\mathcal{M}_θ^G		$\mathcal{M}_\theta^{P_i}$		$\mathcal{A}(\mathcal{M}_\theta^{P_i}, C) - \mathcal{A}(\mathcal{M}_\theta^G, C)$		Model	\mathcal{M}_θ^G		$\mathcal{M}_\theta^{P_i}$		$\mathcal{A}(\mathcal{M}_\theta^{P_i}, C) - \mathcal{A}(\mathcal{M}_\theta^G, C)$	
User	C_a	C_u	C_a	C_u	C_a	C_u	User	C_a	C_u	C_a	C_u	C_a	C_u
61	78.69	69.83	82.59	69.66	+3.9	-0.17	61	76.43	80.00	87.24	73.44	+10.81	-6.56
7C	78.91	76.41	88.00	71.63	+9.09	-4.78	7C	75.07	92.32	83.18	89.39	+8.11	-2.93
80	55.84	26.24	82.36	38.87	+26.52	+12.63	80	54.40	88.77	84.49	81.12	+30.09	-7.65
9D	73.74	85.63	82.81	84.72	+9.07	-0.91	9D	75.58	75.02	82.58	74.65	+7.00	-0.37
B7	56.06	88.33	89.50	86.97	+33.44	-1.36	B7	59.73	84.58	95.56	77.01	+35.83	-7.57
Average					+16.40	+1.08	Average					+18.37	-5.02
Δ_P						+17.49	Δ_P						+13.35

(e) Scenario 1 for Stress Sensing - single context change						(f) Scenario 2 for Stress Sensing - single context change							
Model	\mathcal{M}_θ^G		$\mathcal{M}_\theta^{P_i}$		$\mathcal{A}(\mathcal{M}_\theta^{P_i}, C) - \mathcal{A}(\mathcal{M}_\theta^G, C)$		Model	\mathcal{M}_θ^G		$\mathcal{M}_\theta^{P_i}$		$\mathcal{A}(\mathcal{M}_\theta^{P_i}, C) - \mathcal{A}(\mathcal{M}_\theta^G, C)$	
User	C_a	C_u	C_a	C_u	C_a	C_u	User	C_a	C_u	C_a	C_u	C_a	C_u
1	88.39	81.90	94.54	97.59	+6.15	+15.69	1	66.54	64.71	92.38	94.54	+25.84	+29.83
2	47.40	50.0	77.12	90.47	+29.72	+40.47	2	69.10	50.70	85.26	89.65	+16.16	+38.95
3	36.90	43.48	96.36	95.31	+59.46	+51.93	3	4.76	11.94	74.40	87.28	+69.64	+75.34
Average					+31.78	+36.03	Average					+37.21	+48.04
Δ_P						+67.81	Δ_P						+85.25

(g) Scenario 1 for Stress Sensing - double context change						(h) Scenario 2 for Stress Sensing - double context change							
Model	\mathcal{M}_θ^G		$\mathcal{M}_\theta^{P_i}$		$\mathcal{A}(\mathcal{M}_\theta^{P_i}, C) - \mathcal{A}(\mathcal{M}_\theta^G, C)$		Model	\mathcal{M}_θ^G		$\mathcal{M}_\theta^{P_i}$		$\mathcal{A}(\mathcal{M}_\theta^{P_i}, C) - \mathcal{A}(\mathcal{M}_\theta^G, C)$	
User	C_a	C_u	C_a	C_u	C_a	C_u	User	C_a	C_u	C_a	C_u	C_a	C_u
1	88.39	64.71	94.54	76.46	+6.15	+11.75	1	66.54	81.90	92.38	91.07	+25.84	+9.17
2	47.40	50.70	77.12	63.22	+29.72	+12.52	2	69.10	50.00	85.26	62.84	+16.16	+12.84
3	36.90	11.94	96.36	55.48	+59.46	+43.54	3	4.76	43.47	74.40	87.45	+69.64	+43.98
Average					+31.78	+22.60	Average					+37.21	+22.00
Δ_P						+54.38	Δ_P						+59.21

Table 9. Detailed Personalization (Δ_P) results for WIDAR, ExtraSensory and Stress Sensing dataset

13.08 for Scenario 1 and Scenario 2, respectively, for single context change. Similar personalization benefits could be seen for double context change.

PERCEPT-R: As observed in Table 11b, the variability in generalization benefits among different individuals is less pronounced as compared to personalization benefits. On average, *CRoP* introduces a generalization benefit of 2.57%.

On average over all the datasets, a generalization benefit (Δ_G) of 7.78% percent points are seen over the *conventionally-finetuned* personalized models across all datasets under both scenarios.

B.3 Error Bars

Tables 12a - 12i shows person-wise standard deviation values for generic \mathcal{M}_θ^G , conventionally finetuned $\mathcal{M}_\theta^{C_i^a}$ and *CRoP* $\mathcal{M}_\theta^{P_i^a}$ models.

(a) Scenario 1 for WIDAR dataset													
Model	$M_{\theta}^{C_i^a}$		$M_{\theta}^{P_i^a}$		$\mathcal{A}(M_{\theta}^{P_i^a}, C) - \mathcal{A}(M_{\theta}^{C_i^a}, C)$		Model	$M_{\theta}^{C_i^a}$		$M_{\theta}^{P_i^a}$		$\mathcal{A}(M_{\theta}^{P_i^a}, C) - \mathcal{A}(M_{\theta}^{C_i^a}, C)$	
User	C_a	C_u	C_a	C_u	C_a	C_u	User	C_a	C_u	C_a	C_u	C_a	C_u
0	87.06	65.02	83.67	69.53	-3.38	+4.5	0	77.30	57.46	82.59	58.38	+5.29	+0.92
1	89.38	44.38	86.41	54.45	-2.97	+10.07	1	93.75	42.38	92.45	47.90	-1.30	+5.51
2	75.39	53.19	77.02	62.63	+1.63	+9.44	2	87.15	40.19	87.5	42.31	+0.34	+2.13
Average					-1.57	+8.01	Average					+1.44	+2.85
Δ_G						+6.43	Δ_G						+4.30
(c) Scenario 1 for ExtraSensory dataset													
Model	$M_{\theta}^{C_i^a}$		$M_{\theta}^{P_i^a}$		$\mathcal{A}(M_{\theta}^{P_i^a}, C) - \mathcal{A}(M_{\theta}^{C_i^a}, C)$		Model	$M_{\theta}^{C_i^a}$		$M_{\theta}^{P_i^a}$		$\mathcal{A}(M_{\theta}^{P_i^a}, C) - \mathcal{A}(M_{\theta}^{C_i^a}, C)$	
User	C_a	C_u	C_a	C_u	C_a	C_u	User	C_a	C_u	C_a	C_u	C_a	C_u
61	88.99	68.09	82.59	69.66	-6.40	+1.57	61	93.90	64.27	87.24	73.47	-6.66	+9.17
7C	92.58	61.74	88.0	71.63	-4.58	+9.89	7C	89.19	57.13	83.13	89.39	-6.01	+32.26
80	86.51	49.82	82.36	38.87	-4.14	-10.95	80	89.34	70.23	84.49	81.12	-4.85	+10.89
9D	88.89	83.14	82.81	84.73	-6.07	+1.58	9D	85.53	72.95	82.58	74.65	-2.95	+1.7
B7	95.44	64.19	89.50	86.97	-5.94	+22.78	B7	97.30	67.99	95.56	77.01	-1.74	+9.02
Average					-5.43	+4.97	Average					-4.44	+12.61
Δ_G					-0.46		Δ_G						+8.17
(e) Scenario 1 for Stress Sensing - single context change													
Model	$M_{\theta}^{C_i^a}$		$M_{\theta}^{P_i^a}$		$\mathcal{A}(M_{\theta}^{P_i^a}, C) - \mathcal{A}(M_{\theta}^{C_i^a}, C)$		Model	$M_{\theta}^{C_i^a}$		$M_{\theta}^{P_i^a}$		$\mathcal{A}(M_{\theta}^{P_i^a}, C) - \mathcal{A}(M_{\theta}^{C_i^a}, C)$	
User	C_a	C_u	C_a	C_u	C_a	C_u	User	C_a	C_u	C_a	C_u	C_a	C_u
1	91.17	92.15	94.54	97.59	+3.37	+5.44	1	92.37	96.46	92.38	94.54	+0.01	-1.93
2	68.93	82.81	77.12	90.48	+8.19	+7.67	2	75.57	72.47	85.26	89.65	+9.69	+17.18
3	84.78	90.13	96.36	95.31	+11.58	+5.18	3	64.86	82.52	74.40	87.28	+9.54	+4.76
Average					+7.71	+6.10	Average					+6.41	+6.67
Δ_G						+13.81	Δ_G						+13.08
(g) Scenario 1 for Stress Sensing - double context change													
Model	$M_{\theta}^{C_i^a}$		$M_{\theta}^{P_i^a}$		$\mathcal{A}(M_{\theta}^{P_i^a}, C) - \mathcal{A}(M_{\theta}^{C_i^a}, C)$		Model	$M_{\theta}^{C_i^a}$		$M_{\theta}^{P_i^a}$		$\mathcal{A}(M_{\theta}^{P_i^a}, C) - \mathcal{A}(M_{\theta}^{C_i^a}, C)$	
User	C_a	C_u	C_a	C_u	C_a	C_u	User	C_a	C_u	C_a	C_u	C_a	C_u
1	91.17	72.10	94.544	76.46	+3.37	+4.36	1	92.37	87.22	92.38	91.07	+0.01	+3.85
2	68.93	64.13	77.12	63.22	+8.19	-0.91	2	75.57	59.41	85.26	62.84	+9.69	+3.43
3	84.78	46.06	96.36	55.48	+11.58	+9.42	3	64.86	83.49	74.40	87.45	+9.54	+3.75
Average					+7.71	+4.29	Average					+6.41	+3.75
Δ_G						+12.00	Δ_G						+10.16
(h) Scenario 2 for Stress Sensing - double context change													

Table 10. Detailed Generalization (Δ_G) results for WIDAR ExtraSensory and Stress Sensing datasets

(a) Personalization for PERCEPT-R

Model	M_θ^G		$M_\theta^{P_i}$		$\mathcal{A}(M_\theta^{P_i}, C) - \mathcal{A}(M_\theta^G, C)$	
User	C_a	C_u	C_a	C_u	C_a	C_u
17	72.72	60.51	73.30	63.19	+0.58	+2.68
25	96.79	87.16	96.30	86.83	-0.49	-0.33
28	55.22	54.88	67.12	60.17	+11.90	+5.29
336	100	82.03	100	66.69	0	-15.34
344	77.54	67.48	81.9	65.36	+4.36	-2.12
361	63.63	89.93	64.28	81.73	+0.64	-8.2
362	59.03	66.23	78.52	82.51	+19.49	+16.28
55	95.77	85.34	97.14	80.41	+1.38	-4.93
586	65.85	58.25	73.17	65.87	+7.32	+7.62
587	64.71	65.1	69.4	65.19	+4.68	+0.09
589	66.34	60.87	63.69	62.77	-2.64	+1.90
590	69.05	61.04	71.08	73.26	+2.03	+12.22
591	61.91	58.68	72.03	63.44	+10.12	+4.76
61	72.86	69.42	77.78	66.66	+4.92	-2.76
67	80.12	77.64	81.00	72.48	+0.89	-5.15
80	89.38	85.54	91.22	87.87	+1.85	+2.33
Average					+4.19	+0.90
Δ_P					+5.09	

(b) Generalization for PERCEPT-R

Model	$M_\theta^{C_i}$		$M_\theta^{P_i}$		$\mathcal{A}(M_\theta^{P_i}, C) - \mathcal{A}(M_\theta^{C_i}, C)$	
User	C_a	C_u	C_a	C_u	C_a	C_u
17	70.56	60.17	73.30	63.19	+2.74	+3.01
25	94.91	83.8	96.30	86.83	+1.39	+3.03
28	64.81	58.84	67.12	60.17	+2.31	+1.33
336	100	60.79	100	66.69	+0	+5.90
344	82.77	64.68	81.9	65.36	-0.88	+0.68
361	57.61	78.66	64.28	81.73	+6.67	+3.07
362	75.44	82.9	78.52	82.51	+3.08	-0.39
55	100	76.86	97.14	80.41	-2.86	+3.55
586	70.94	64.46	73.17	65.87	+2.23	+1.41
587	70.84	66.23	69.4	65.19	-1.44	-1.04
589	67.26	60.59	63.69	62.77	-3.57	+2.18
590	67.76	70.54	71.08	73.26	+3.32	+2.73
591	71.83	64.2	72.03	63.44	+0.20	-0.76
61	74.93	65.23	77.78	66.66	+2.86	+1.43
67	79.83	74.16	81.00	72.48	+1.18	-1.68
80	89.31	90.33	91.22	87.87	+1.92	-1.68
Average					+1.20	+1.37
Δ_G						+2.57

Table 11. Detailed Personalization (Δ_P) and Generalization (Δ_G) results for PERCEPT-R datasets

(a) Scenario 1 for WIDAR dataset

Model	\mathcal{M}_θ^G		$\mathcal{M}_\theta^{P_i^a}$		$\mathcal{M}_\theta^{C_i^a}$	
User	C_a	C_u	C_a	C_u	C_a	C_u
0	2.17	0.88	3.69	0.49	2.09	0.29
1	1.49	1.73	1.94	2.97	0.70	1.94
2	3.61	0.68	4.28	5.50	3.8	2.31

(b) Scenario 2 for WIDAR dataset

Model	\mathcal{M}_θ^G		$\mathcal{M}_\theta^{P_i^a}$		$\mathcal{M}_\theta^{C_i^a}$	
User	C_a	C_u	C_a	C_u	C_a	C_u
0	2.67	1.60	1.83	0.95	1.02	0.41
1	1.58	0.64	2.29	0.97	2.22	0.68
2	2.49	0.19	0.79	0.56	1.72	0.39

(c) Scenario 1 for ExtraSensory dataset

Model	\mathcal{M}_θ^G		$\mathcal{M}_\theta^{P_i^a}$		$\mathcal{M}_\theta^{C_i^a}$	
User	C_a	C_u	C_a	C_u	C_a	C_u
61	2.63	0	4.14	1.65	3.28	2.52
7C	1.45	0	1.17	0.81	1.36	0.83
80	0.42	0	4.17	3.04	2.81	1.44
9D	0.30	0	2.58	1.08	2.53	0.94
B7	0.74	0	3.02	7.28	2.13	3.48

(e) Scenario 1 for Stress Sensing - single context change

Model	\mathcal{M}_θ^G		$\mathcal{M}_\theta^{P_i^a}$		$\mathcal{M}_\theta^{C_i^a}$	
User	C_a	C_u	C_a	C_u	C_a	C_u
1	3.55	0	5.78	4.53	7.94	6.17
2	5.13	0	14.65	3.71	8.74	10.49
3	17.61	0	8.17	4.79	15.95	3.45

(g) Scenario 1 for Stress Sensing - double context change

Model	\mathcal{M}_θ^G		$\mathcal{M}_\theta^{P_i^a}$		$\mathcal{M}_\theta^{C_i^a}$	
User	C_a	C_u	C_a	C_u	C_a	C_u
1	3.55	0	5.75	3.33	7.94	4.78
2	5.13	0	14.66	10.19	8.74	8.70
3	17.61	0	8.17	5.52	15.95	3.58

(d) Scenario 2 for ExtraSensory dataset

Model	\mathcal{M}_θ^G		$\mathcal{M}_\theta^{P_i^a}$		$\mathcal{M}_\theta^{C_i^a}$	
User	C_a	C_u	C_a	C_u	C_a	C_u
61	3.93	0	4.03	2.67	4.72	1.00
7C	2.45	0	2.35	2.50	2.85	0.45
80	3.33	0	0.65	3.09	1.30	1.01
9D	4.18	0	3.22	0.88	5.54	0.80
B7	3.13	0	0.83	3.27	0.24	2.79

(f) Scenario 2 for Stress Sensing - single context change

Model	\mathcal{M}_θ^G		$\mathcal{M}_\theta^{P_i^a}$		$\mathcal{M}_\theta^{C_i^a}$	
User	C_a	C_u	C_a	C_u	C_a	C_u
1	4.95	0	3.02	0.66	3.02	2.34
2	13.68	0	2.67	7.82	11.51	5.58
3	8.25	0	21.02	7.00	17.89	6.57

(h) Scenario 2 for Stress Sensing - double context change

Model	\mathcal{M}_θ^G		$\mathcal{M}_\theta^{P_i^a}$		$\mathcal{M}_\theta^{C_i^a}$	
User	C_a	C_u	C_a	C_u	C_a	C_u
1	4.95	0	3.02	3.00	3.02	2.52
2	13.68	0	2.67	5.62	11.51	0.60
3	8.25	0	21.02	2.23	17.89	2.07

(i) PERCEPT-R

Model	\mathcal{M}_θ^G		$\mathcal{M}_\theta^{P_i^a}$		$\mathcal{M}_\theta^{C_i^a}$	
User	C_a	C_u	C_a	C_u	C_a	C_u
17	7.17	0	9.75	1.64	4.18	1.11
25	1.34	0	2.35	2.20	2.29	0.85
28	3.38	0	15.16	0.85	15.14	0.60
336	0	0	0	7.25	0	5.64
344	5.50	0	4.86	1.13	4.10	1.87
361	15.75	0	13.18	3.96	12.44	6.39
362	3.10	0	7.59	4.46	4.53	4.83
55	3.75	0	0	3.32	2.58	2.77
586	4.01	0	1.09	1.77	3.26	0.22
587	3.06	0	4.24	1.20	5.48	1.43
589	0.45	0	2.33	2.72	1.44	0.94
590	2.26	0	3.20	2.17	5.58	0.57
591	3.36	0	3.11	1.11	3.91	0.74
61	9.30	0	6.33	2.37	5.05	1.67
67	5.50	0	3.59	2.20	3.11	2.38
80	6.11	0	4.29	1.61	5.69	0.68

Table 12. Standard Deviation for Generic, conventionally finetuned and CRoP models for WIDAR, ExtraSensory and Stress Sensing dataset